2012

Technical feasibility of storage on large dish stirling systems

Charles E. Andraka

K Scott Rawlinson

Nathan P. Siegel
Bucknell University

SANDIA REPORT
SAND2012-8352
Unlimited Release
Printed September 2012

Technical Feasibility of Storage on Large Dish Stirling Systems

Charles E. Andraka
K. Scott Rawlinson
Nate P. Siegel

Prepared by
Sandia National Laboratories
Albuquerque, New Mexico 87185 and Livermore, California 94550

Sandia National Laboratories is a multi-program laboratory managed and operated by Sandia Corporation, a wholly owned subsidiary of Lockheed Martin Corporation, for the U.S. Department of Energy's National Nuclear Security Administration under contract DE-AC04-94AL85000.

Issued by Sandia National Laboratories, operated for the United States Department of Energy by Sandia Corporation.

Available to DOE and DOE contractors from
U.S. Department of Energy
Office of Scientific and Technical Information
P.O. Box 62
Oak Ridge, TN 37831

Telephone: (865) 576-8401
Facsimile: (865) 576-5728
E-Mail: reports@adonis.osti.gov
Online ordering: http://www.osti.gov/bridge

Available to the public from
U.S. Department of Commerce
National Technical Information Service
5285 Port Royal Rd.
Springfield, VA 22161

Telephone: (800) 553-6847
Facsimile: (703) 605-6900
E-Mail: orders@ntis.fedworld.gov
Online order: http://www.ntis.gov/help/ordermethods.asp?loc=7-4-0#online

SAND2012-8352
Unlimited Release
Printed September 2012

Technical Feasibility of Storage on Large Dish Stirling Systems

Charles E Andraka
Concentrating Solar Technologies

K. Scott Rawlinson
Satellite Mechanical Design

Sandia National Laboratories
PO Box 5800 MS 1127
Albuquerque, NM 87185-1127

Nate P. Siegel
Bucknell University
1 Dent Drive
Lewisburg, PA 17837

Abstract

Dish-Stirling systems have been demonstrated to provide high-efficiency solar-only electrical generation, holding the world record at 31.25%. This high efficiency results in a system with a high possibility of meeting the DOE SunShot goal of $0.06/kWh. Current dish-Stirling systems do not incorporate thermal storage. For the next generation of non-intermittent and cost-competitive solar power plants, we propose a thermal energy storage system that combines latent (phase-change) energy transport and latent energy storage in order to match the isothermal input requirements of Stirling engines while also maximizing the exergetic efficiency of the entire system.

This report takes an initial look at the technical advantages of dish Stirling with storage as well as the technical challenges, in order to make a preliminary estimate as to the technical feasibility of such a system.

We find that a storage system using metallic eutectic phase change storage results in a feasible physical embodiment, with mass, volume, and complexity suitable for 25kWe dish Stirling systems. The results indicate a system with 6 hours of storage and a solar multiple of 1.25 provides the optimum impact to LCOE and profit. Further, for no negative impact on LCOE, the optimal storage system may cost as much as $82/kWhth or $33k/dish, a substantial departure from the SunShot goals for tower systems. The storage system also is shown to have substantial structural benefits to the dish design. In addition, there may be benefits in terms of capacity payments or failure-to-deliver penalties. A dish storage system design must take into account the value placed on storage by the PUC or utility.

Acknowledgments

This report was made possible through funding from the U.S. Department of Energy_s (DOE_s) Energy Efficiency and Renewable Energy program. To learn more, please visit energy.sandia.gov and http://www.eere.energy.gov . We also wish to acknowledge the leadership offered by Joe Stekli of DOE_s Solar Energy Technology Program. We would like to thank personnel from Sandia National Laboratories, for their encouragement of this document. In addition, we would like to thank the multitude of reviewers that took the time to edit and contribute to this document.

Contents

Figures

Tables

Acronyms

AE – Annual Energy
CC – Capital Cost
CCWS – Capital Cost With Storage
CSP – Concentrating Solar Power
DIR – Directly Illuminated Receiver
DOE – US Department of Energy
EM – Electro Magnetic
FCR – Fixed Charge Rate
FOA – Funding Opportunity Announcement
IPP – Initiative for Proliferation Prevention, a DOE program employing former Soviet scientists
JPL – Jet Propulsion Lab
KPI – Kiev Polytechnic Institute
kW_e – kilowatt electric
kW_t – kilowatt thermal
LCOE – Levelized Cost of Energy
NSTTF – National Solar Thermal Test Facility
RPPD – Rated Power Per Dish
SM – Solar Multiple
SVC – Storage Variable Cost
TES – Thermal Energy Storage
TOD – Time of Delivery

This page intentionally left blank

1 BACKGROUND

1.1 Dish Technology

Dish engine systems are point-focus "distributed" systems, typically sized for 3 to 30 kW of electrical output. Some industry partners have determined that large single-site deployments of dish systems can lead to utility-scale implementations with a cost-effective deployment [1,2]. The dish systems are two-axis tracking, point focus systems with geometric concentration ratios (at the aperture) of typically 3000:1. The dish systems typically have a high percentage of their cost in the dish, and the facets may be costly to manufacture due to the tight curvature required.

Typical dish systems are a "balanced" system with a pedestal drive, Figure 1. The pedestal drive system allows the loads to be brought to a central location, minimizing point loading on the periphery of the dish seen on other drive configurations. The engine package is typically quite heavy, and extended on a boom in front of the dish. In order to reduce drive loads, the system is nearly balanced at the elevation pivot, which is in front of the dish surface. This in turn requires a "slot" in the dish reflective surface to accommodate the drive support pedestal. This slot reduces the strength of the dish structure. Most current typical dishes consist of a steel back structure, with independent facets mounted to the steel frame and adjusted to "align" the dish.

Figure 1. McDonnell Douglas dish, showing typical balanced configuration.

1.2 Stirling Technology

The engine of choice for dish-engine systems is the Stirling Cycle engine. The ideal Stirling cycle has an area equivalent to the Carnot cycle on the temperature-Entropy diagram (T-S diagram), and thus can approach the ideal system performance more than other practical thermodynamic cycles. The Stirling Cycle features isothermal input (3-4 on Figure 2), unlike Brayton or Rankine cycles which require sensible heating at the input. Practical Stirling cycle engines are available with input temperatures approaching 800°C, allowing high efficiency externally-heated engines.

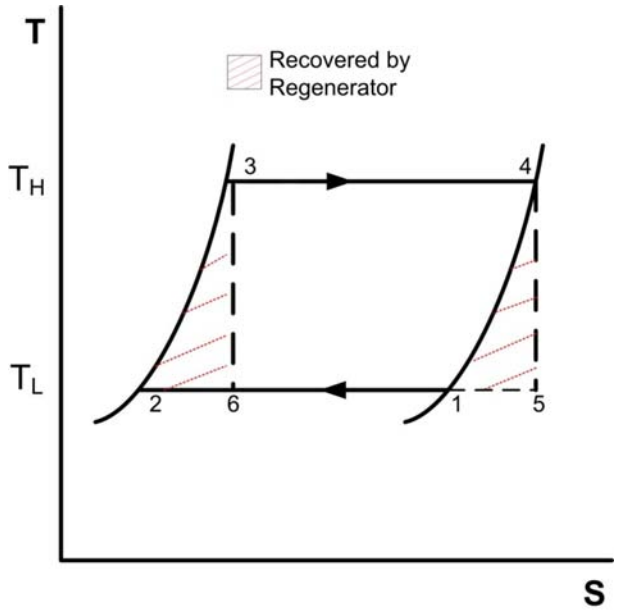

Figure 2. Temperature-Entropy diagram comparing the Ideal Stirling Cycle (1,2,3,4) and Ideal Carnot Cycle(5,6,3,4).

Dish-Stirling systems have been demonstrated to provide high efficiency solar-only electricity generation, holding the world record at 31.25% net conversion from sunlight to 3-phase grid power. This high efficiency results in a system with a high possibility of meeting the DOE SunShot goal of $0.06/kWh. Current dish-Stirling systems do not incorporate thermal storage, but operate only when the sun is shining. The receiver of the Stirling cycle is typically a bundle of tubes through which the engine working fluid, hydrogen or helium, shuttles back and forth. The engine typically has little thermal inertia, with a cold startup to full power completed in several minutes rather than hours. Conversely, upon loss of solar input (clouds or sunset), the output is diminished rapidly.

Dish systems with high concentration result in a bright spot (glare), which is also an attractive nuisance. Anything placed into the focal region immediately bursts into flame or melts. Therefore, it is likely that dish Stirling systems will only be deployed in access-controlled areas, leading to larger installations rather than disperse deployments. In these large installations, dish-to-dish shading is important. A Sandia National Laboratories study [3] indicated that the Stirling Energy Systems (SES) system could operate to about 10.5% shading, after which unbalanced cylinder operation caused a controls trip on the engine. In a large field, shading in the morning, evening, and noon near the Winter solstice resulted in a loss of 5-6%

of the generation compared to a standalone system. A heat pipe receiver could increase the allowable shading fraction, and therefore increase the annual energy capture of the system.

However, the same study indicates that dish-Stirling takes good advantage of the lucrative summer afternoon bonus offered by Southern California Edison and other utilities in their rate structure. The current rate structures put little premium on the evening hours, and the Solar-only Stirling systems operated through much of the peak value hours. Other California utilities have similar Time of Delivery (TOD) rate structures, though none favor the afternoon as strongly as SCE. None of the TOD schedules give significant emphasis to evening generation.

SES indicated that they planned to install systems in large fields at $2-3/W [1], and the 25kW rated system would generate about 56MW-hr/year. With a fixed charge rate of 7.42% [4] and O&M at $0.045/W/year, the projected LCOE is $0.085/kWh. Using the current SCE TOD rate structure [5] and a base price of $0.10/kWh, the effective value of the system (sales value of the energy generated, averaged over the year) is $0.14/kWh.

The dish Stirling systems, as presented by SES [6], have the potential for reaching SunShot goals ($0.06/kWh) with supply chain development, design for manufacture, and offshore sourcing. This is without any difficult technical challenges. Onshore manufacture was anticipated to add about $0.02/kWh.

This report will explore the feasibility of adding significant storage to the SES-sized dish Stirling systems. While not exhaustive, the results of this report should guide next-generation development to provide a system that not only matches Photovoltaic‘s projected price performance, but also incorporates significant thermal storage to ride through transients and extend capacity.

This page intentionally left blank

2 PROPOSED STORAGE FOR DISH STIRLING

2.1 Introduction

For the next generation of non-intermittent and cost-competitive solar power plants, we propose a thermal energy storage system that combines latent-energy transport and latent-energy storage in order to maximize the exergetic efficiency of the entire system. We propose a configuration that allows implementation on the movable portion of the dish—eliminating the need for high-temperature rotating or flexible joints and minimizing heat losses in thermal transport. In addition, we propose using Sandia-developed high-performance heat pipes that allow extension of storage to large (25 kW_e) systems. This configuration was originally proposed as an ARPAe HEATS project [7]

Our proposed configuration centers on providing transport that enables storage and engine mounting on the rear of the dish rather than at the focus. This allows a substantially higher thermal storage mass than can be supported on the power conversion unit (PCU) boom, facilitating storage durations of six or more hours. Figure 3 schematically shows the proposed system layout (not to scale: The dish is typically 11-12m in diameter. The proposed storage media is approximately $1m^3$). A pumped condensate heat pipe transports energy from the solar receiver to the storage media nearly isothermally. The storage media is a salt or metallic Phase Change Material (PCM), for high-density isothermal storage. A second isothermal heat pipe transports the thermal energy from storage to the engine, providing high flux to the engine through condensation. The separate heat pipe systems provide a "thermal diode" effect to reduce losses when operating from stored energy.

The proposed approach leverages the existing high-temperature (700–800 °C), high efficiency system, and provides a storage option. In contrast, in order to approach SunShot goals, trough and tower high-temperature storage systems need further development to provide a high-temperature thermodynamic cycle and receiver, as well as high-concentration optics suitable to limit collection losses.

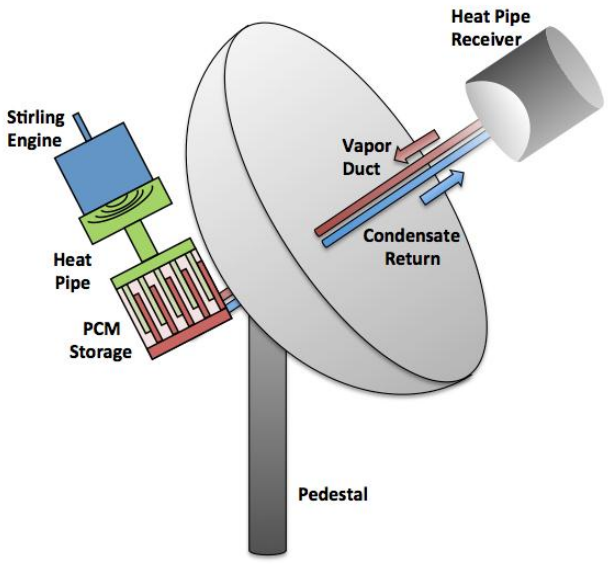

Figure 3. Schematic of proposed latent energy storage system for dish-Stirling

The proposed development work includes developing and demonstrating high-performance interfaces throughout the proposed system. A successful system design includes proving and characterizing these interfaces. The first interface is the solar-to-heat pipe (receiver), which requires a high performance robust wick system to properly distribute the heat transport fluid to the receiver. The second interface is the heat-pipe-condenser-to-storage-media. This interface requires a thorough understanding of the dynamic heat-transfer characteristics at various stages of PCM melt. The third interface is similar to the second, involving the energy transport out of storage and into the secondary heat pipe vapor space. Finally, we must consider the interface with the engine, which is highly design-specific, but for test purposes we will simulate this with gas-gap calorimeters to accurately characterize heat transfer rates.

Sandia is a recognized leader in dish-Stirling technology development. Sandia developed very high performance heat-pipe receivers in the 1990s and demonstrated operation with a Stirling system on sun [8]. Sandia has also performed as the lead lab on thermal storage technologies for CSP and has expertise in storage media formulation, for both sensible and latent storage systems. Being one of the nation‘s lead weapons laboratories, Sandia also has key expertise in long-term materials compatibility, a key area for storage systems. We can leverage expertise throughout Sandia to support this project as needed.

The proposed system takes the highest performance solar electric generation system and moves it to the realm of intermediate, non-intermittent power generation. This expands the capability of the systems with the best chance of meeting the aggressive SunShot levelized cost of energy (LCOE) goals, without needing complimentary programs to develop other high-temperature, high-performance subsystems.

2.2 Technical Feasibility Issues

When considering latent transport (heat pipe receiver), we must consider both the physical and thermal sizing of the heat pipe absorber. The transport liquid distribution system (wick structure) requirements scale with the peak concentrated thermal flux, the total thermal power throughput, and the areal extent and height of the capillary wicking structure. Therefore, a suitable heat pipe for a 3 kW_e system (10 kW_{th}) may not provide the wick capability needed for a 25 kW_e (70 kW_{th}) system. The addition of storage, with a solar multiple (increased reflective surface area), will further increase the wick requirements. This work will focus on the 25kW_e system scale.

An important difference between Stirling engine systems and typical Rankine cycle or Brayton cycle systems is that the heat input to the engine is isothermal. While this leads to high engine efficiency, it means that if sensible heat is used to transport the concentrated solar energy to the engine, significant second-law losses will entail. This is because the source (transport fluid) must be hotter than the input surface of the engine in order to transport energy into the engine and therefore the heat cannot be removed below this temperature. Because sensible heat requires a temperature change, the transport fluid must start out significantly hotter than the input surface such that sufficient energy can be imposed before the fluid drops to the input temperature. This results in large exergy losses (Figure 4). With a Stirling-cycle engine, if a flux boundary condition (Directly Illuminated Receiver (DIR)) or an isothermal boundary condition (latent transport) is provided to the engine, the exergy losses are limited to the heat transfer coefficients for conduction through heat exchanger materials and convection into the working fluid.

Sandia has performed significant development on heat pipe receivers [9,10], and has demonstrated very high peak flux and total power performance without artery structures. Arteries can be used in heat pipes to provide bulk fluid distribution over the wick. However, an artery is similar to lifting fluid with a soda straw. Once the prime is lost in an artery, it ceases to function, and repriming may not be a passive operation. While industry-designed heat pipes were demonstrated with high throughput (115 kW_{th}), they did so at lower flux levels (requiring larger areal extents, therefore more material) and with the assistance of an artery structure. Sandia developed and demonstrated high-performance wicks, using felt metal wick technologies. Further demonstration testing must be performed to validate potential robust felt wick solutions that bypass observed durability limitations of the Sandia felt wicks [11].

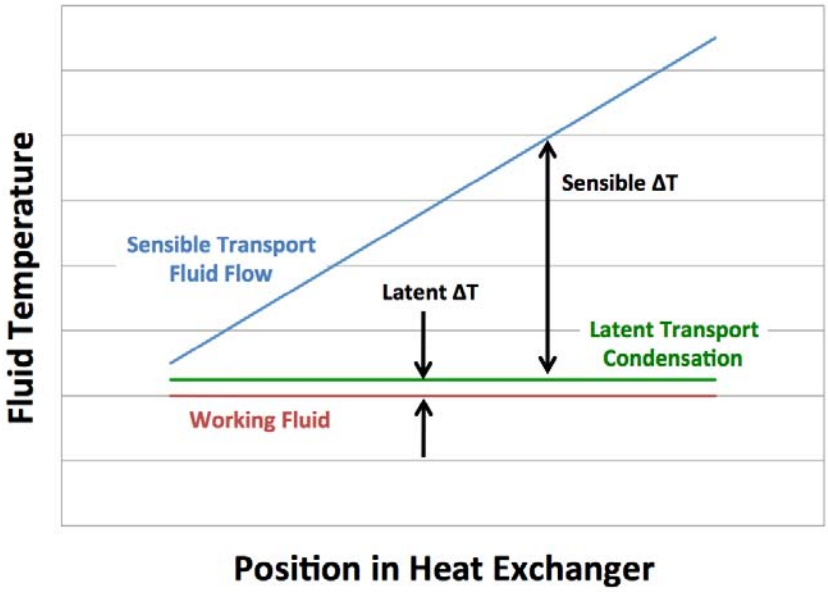

Figure 4. Comparison of sensible and latent heat transport into a Stirling engine.

A key finding in prior Sandia work was that a heat pipe (no storage) resulted in a 20% performance enhancement over a DIR on an STM 4-120 Stirling engine [8]. The primary reasons for this were two-fold. First, the receiver is limited in peak temperature for material strength reasons. With direct illumination, individual tube temperatures were driven by local flux and the net output gas temperature was driven by the average tube temperature. In the case of a heat pipe, the heat transfer is nearly isothermal, so the average temperature rises to approach the peak temperature. This results in a substantial increase in the hot-end working gas temperature, improving efficiency. In addition, because heat is applied around the entire circumference of the tube, rather than to one side of the tube, the length of the tube can be reduced while maintaining the same effective heat transfer area. A reduction in tube length reduces the —dead volume" of the engine and increases the compression ratio, which is known to enhance the system efficiency. The substantial improvement in engine performance, both in first law and second law terms, can offset the slight second law inefficiencies in the proposed transport system.

2.3 Innovations of Proposed Work

The proposed method of thermal storage on a dish-Stirling system has many significant improvements over the current state-of-the-art. These technical advantages and innovations make this effort worth pursuing despite the technical challenges.

2.3.1 Innovation 1: High Operating Temperature

Current technology Stirling engines have surface temperature approaching 800 °C with working fluid temperature of 650 °C or higher. Because the heat rejection temperature is close to ambient, the Stirling engine has excellent exergetic and first law efficiencies. The Stirling cycle also closely matches the ideal Carnot cycle, which defines the maximum work available from a thermodynamic cycle. Figure 2 shows the Temperature-Entropy plot for the ideal Stirling Cycle (1,2,3,4) overlaid on the ideal Carnot Cycle (5,6,3,4). The area enclosed within the cycle is proportional to the power generated, and is equivalent in the Stirling and Carnot cases for given temperature and entropy ranges. Thermal energy is input and exhausted in the isothermal lines of the cycle. Our proposal builds upon existing high temperature, high performance engines and optical systems, rather than relying on yet-to-be-developed thermodynamic cycles and high temperature systems.

2.3.2 Innovation 2: Isothermal Storage and Heat Transport

Exergetic losses are minimized when a thermal storage system is closely matched to the thermodynamic cycle. The Stirling cycle uses isothermal heat input. Therefore phase-change (latent) storage and phase-change heat transport processes, both of which are isothermal processes, can provide a source temperature that matches the needs of the engine. This match limits the exergetic losses of the system as compared to utilizing sensible storage or heat transport.

2.3.3 Innovation 3: High Exergetic Efficiency

The isothermal nature of the storage, transport, and transfer of energy to the engine leads to high exergetic efficiency. The primary second-law loss is in the temperature drop through conduction into and out of the PCM storage media. This temperature drop can be tuned against costs by optimizing the number, size, and configuration of the heat-pipe condensers and evaporators in the PCM container. The transport is by saturated vapor, so there is little temperature drop in transport, given sufficient vapor passage diameter. If the entire thermal system is considered, we see a system-level exergetic benefit of 4–8 percentage points (a substantial improvement) over a direct illumination receiver despite the addition of transport and storage to the system.

2.3.4 Innovation 4: Storage Behind the Concentrator

Current dish-Stirling designs typically have the engine positioned on a boom on the sun side of the concentrator. This proximity reduces thermal losses through short transport distances. Past concepts for thermal storage have either (1) put small amounts of thermal storage on the end of the boom at the engine for short duration storage or (2) put storage on the ground, which requires very long transport distances and complicated, high-cost, high-temperature rotary joints around the tracking pivots. With the high-efficiency heat transport capabilities of heat pipes, we propose to have the receiver on a small, lightweight boom near the focus and bring the thermal energy to the back side of the concentrator in a high-performance heat pipe.

Having the thermal storage and engine on the back of the concentrator has many advantages. First, the storage volume/thermal capacity can be much greater than in a boom-mounted storage system—where the strength of the boom is a cost issue. We can achieve a storage capacity comparable to a ground-mounted system without the complexity, thermal loss, and expense of rotary joints. Second, the boom will be lighter and the structure necessary to support the boom will be lighter as well, which will reduce material costs. Third, the center of gravity of the entire system will change, allowing the tracking pivot to be positioned behind the concentrator. This will allow a design that (1) eliminates the pedestal gap typical of a balanced dish-engine system, (2) significantly stiffens the dish support structure, and (3) likely reduces the material required in the dish structure in a substantial way.

2.3.5 Innovation 5: Thermal Diode Effect

A key innovation of the proposed design is the thermal diode achieved by using two heat pipes coupled through the storage system. Other designs have used a single heat pipe from receiver to engine heater head—with the storage tacked on to consume any extra available heat. In a single-heat-pipe system that is discharging from storage when not on sun, some of the heat from storage will go to the heater head *and some will go to back to the receiver*—suffering energy loss not only through conduction from the long heat pipe, but also from radiation and convection at the receiver.

The thermal diode effect is achieved by not supplying liquid sodium to the PCM end of the receiver heat pipe and therefore preventing significant thermal energy from traveling backward through that heat pipe.

2.3.6 Innovation 6: High-Performance Heat Pipes and Spherical Absorber Geometry

Sandia has developed high-performance heat pipes that efficiently transfer large quantities of heat at high flux levels. Sandia development work has especially focused on the wick materials and the effects of pore size distribution, pore connectivity, wick attachment, and innovative multilayer wick structures. Sandia has worked with collaborators to develop wicks that use sintered felt metal, which has a high pore-to-wick-material ratio while still retaining correct pore size distribution and connectivity.

In addition, Sandia has performed research on a spherical absorber geometry, which is better suited to concentrated solar input configurations than a tubular receiver geometry. Such receiver cavity assemblies have demonstrated thermal efficiencies approximately 93%, compared to DIR heater head cavity systems at 85% efficiency [8].

2.3.7 Innovation 7: Heat Pipe Interface to Engine

The design of the solar receiver of a Stirling engine requires a careful assessment of the incoming flux to achieve maximum engine efficiency without exceeding material properties. Current systems position the receiver tubes behind the dish‘s focus and require long heat-exchanger tubes to spread the incoming solar flux over a large tube area to maintain allowable front-side tube temperature. The long tubes introduce dead volume into the engine with a large volume of gas in the tubes instead of in the cylinder where it can produce power through compression and expansion.

Introducing a heat pipe between the receiver and engine heater head offers two significant system improvements. First, the heat pipe automatically balances the thermal input between the different cylinders of the engine. This is necessary to achieve maximum engine efficiency and power throughput.

Second, a conventional receiver absorbs energy on the front side of the heater head tubes, where they are illuminated by the incident radiation. The energy that can be delivered to the tubes depends on the maximum allowable temperature for the tubing material. However, this maximum temperature is only experienced on the front side of the tubes. The result is an engine gas temperature that is as much as 220 °C lower than the highest tube temperature. Using a heat-pipe receiver allows the heater head tubes to absorb energy around the entire outer surface of the tubes, achieving a much larger energy input with much less tube length, as well as a lower temperature drop form the absorber surface to the engine working fluid.

2.3.8 Innovation 8: Thermal Transformer Effect

In a typical solar receiver design for a Stirling engine, the size of the receiver is determined through a balance of incoming radiation, tube material limitations, and the desire to reduce dead volume to increase engine efficiency. In a heat-pipe receiver, the size of the receiver and the size of the heater head are less interdependent. This ―thermal transformer” allows a design that optimizes the size of the receiver to reduce re-radiation and the engine heater head size for optimal engine performance. Certainly, both ends of the heat pipe must incorporate design considerations for vapor creation and condensation, but the thermal transformer greatly increases design space for independent optimization leading to increases in system efficiency.

2.4 Differentiation from Others

One of the shortfalls of dish-engine concentrating solar power has been the lack of storage. This has become ever more apparent as dish-engine systems have sought to distinguish themselves from photovoltaic panels. The addition of 6 hours of storage would make dish Stirling competitive in the mid-load power market and approach baseload power requirements. The highest-performing, highest-efficiency system among the concentrating solar power options is dish-Stirling. The addition of storage and a mechanism for transporting high-temperature heat would introduce high capacity to its benefits.

Current storage systems being developed for dish-Stirling applications can be divided into short- (on the order of 1 hour) and long-term (4+ hours) approaches. Because the mass of the storage media is small for short-term storage, the thermal energy storage system can be co-located with the Stirling engine on the end of boom, simplifying the design. This is the approach that Infinia Corp. is pursuing in one of their Funding Opportunity Announcements (FOAs) on their 3 kW_e system [12]. Infinia is using heat pipes to distribute the heat throughout the phase-change thermal storage unit. However, the short-term storage does not significantly increase the capacity factor and limits applicability for near-baseload energy.

Long-term storage necessitates more storage media, which cannot be accommodated easily on the end of a dish boom due to concerns regarding seismic and wind loading. Infinia Corp. is also investigating long-term storage under a baseload FOA but they have yet to determine a clear path to an appropriate configuration and transfer of heat to the larger storage unit. The current focus is on the internal distribution of heat within the storage container using liquid metals.

Jet Propulsion Laboratory (JPL) reports indicate that adding approximately 6 hours of storage, thereby increasing the capacity factor to 0.5–0.6, could be accomplished with minimal increase in the levelized cost of energy (LCOE) for dish-Brayton [13]. Significant increases in cost are not anticipated until capacity factors reach approximately 0.75 and above. Fujita [14] identifies that a multi-dish cluster using sensible or latent-heat storage system shows promise. They also identify challenges associated with this approach that include materials compatibility, phase-change processes, pumps and valves for molten salt, and high-temperature flex hoses/swivel joints.

A later JPL report proposed and analyzed four possible configurations for dish-Stirling receivers [15]. Of the approaches considered, the indirect coupled thermal energy storage (TES) receiver, where the solar energy is funneled through a TES system en route to the engine heater, demonstrated the most desirable characteristics for high performance, durability and low-cost.

A third JPL report pursued a goal to define a promising alkali metal heat transport and storage system for dish-Stirling [13]. The storage system was 1.7–2 hours of Stirling operation at 52.5 kW and included considerations for TES materials, operating conditions, transport mechanisms and system design. They identified that transporting energy via latent heat in a heat pipe provides a very high thermal conductance with negligible vapor flow pressure making it a nearly isothermal device. Results indicated that latent-heat storage and liquid metal heat pipes (preferably Na) were the desired arrangement.

These JPL reports did not result in hardware or experimental demonstration of the approaches considered. This proposal seeks to capitalize on lessons learned from the above works with several important distinguishing characteristics: long-term storage, high-temperature transport, heat pipe receivers, and latent storage.

2.5 Leapfrog Potential

The innovations noted above lead to a high-performance CSP technology with sufficient storage to provide intermediate or baseload energy production. Tower and trough proposals to meet SunShot objectives with thermal storage require higher temperature operation, which requires development of large, high-temperature thermodynamic cycles, high-temperature receivers, higher-performance optics to minimize losses, as well as high-temperature storage material options. Our proposed work leverages existing high-temperature, high-performance dish-Stirling systems, and incorporates a feasible advanced latent energy storage and transport system. Thus, the development of the storage system leads directly to intermediate and baseload power, without the need for additional, expensive, and long-term development on other major components.

This page intentionally left blank

3 SYSTEMS STUDY

3.1 Introduction

A simplified systems model was developed to explore appropriate sizing and operation of a dish-Stirling storage system, and to evaluate at a high level the impacts on LCOE. The model is intended to explore trends and overall impact, but would need further refinement to be used as a design tool.

The systems level model is used to determine the overall feasibility, defined as impact on the LCOE of the system, of a storage system for dish Stirling. Further, the model provides high-level insights into the sizing requirements. This is particularly important in terms of the heat pipe receiver (solar interface) sizing, as too large a required solar multiple could place the system beyond near-term feasibility.

3.2 Model Description

The model is based on a previous systems model [3], which considers a full field of dish systems, including shading dish to dish. The original model was based on the SES MPP-vintage dish (rectangular facets, "Model Power Plant"), and used measured data to develop the linear operation curve. The model uses either TMY2 data (hourly), or Solergy data (15-minute data) from ground-based measurements. In the case of this study, I used the 15-minute data available from Barstow CA, from 1977 measurements.

The model was modified to support operation with storage. A thermal accumulator was added, with a user-specified capacity per dish. Each dish accumulator was tracked separately, due to edge effects in the field.

The thermal performance of the system was separated from the system performance, based on prior dish Stirling system modeling results [16]. These prior modeling efforts separated the engine performance from the system performance based on thermal modeling of the Direct Illumination Receiver (DIR). However, other prior work [8] indicated that the heat pipe receiver has about 93% thermal efficiency at rated power, while the DIR rated efficiency is only 85%, primarily due to the uncooled ceramic stone in the center of the receiver, which has a large view factor to the environment. In addition, the same prior experimental work indicates that the system performance is enhanced by about $3kW_e$ output, from about $18kW_e$ with a DIR and hydrogen working fluid to $21kW_e$ with a heat pipe receiver and helium working fluid. The modeled thermal performance combined with the measured system performance, led to thermal and system performance characteristics shown in Figure 5. The thermal power required to operate the engine at rated power of $25kW_e$ is reduced from $68.88kW_t$ to $66.65kW_t$ by the use of the heat pipe input.

The thermal input to the engine to operate at various power levels is derived from Figure 5 (thermal and electric power vs. insolation), and is presented in Figure 6. The thermal input received is applied to the accumulator, after any shading effects. The system was allowed to operate through 85% shading, and no additional shading degradation of engine performance was applied. The non-zero x-axis crossing is due to thermal losses that are fixed rather than dependent on power levels, such as thermal re-radiation from the hot receiver. A 2kW constant thermal loss from the PCM storage was applied whenever the storage accumulator contained positive energy.

The storage system and engine operation cycle can be controlled in a variety of ways. One must consider at least the following:

- Engine startup conditions

- Engine operating power levels
- Storage full response

I developed several start criterion. The first is a minimum storage accumulated switch. Once this level is reached, the engine is able to start. I chose 10% for all of the cases studied, but left this as a user input. In addition, I added a time-of-day (TOD) switch, such that the engine would not start until a certain clock time each day. This would allow storage to accumulate, and could be tuned to return the highest value from storage. Finally, if the TOD was not reached, but the storage was nearly full (80% was selected), the engine would start. Anytime the engine starts, it continues to run until storage is depleted. The engine is operated at full rated power (25kW$_e$) whenever it runs, simplifying the control approach. It is assumed that the storage is entirely latent and isothermal delivery to the engine, so that the performance does not change. In reality, some sensible storage would be present, in both filing and depleting storage. Finally, if the storage reaches capacity, with the engine running, then excess thermal energy is ~~"s~~hed" by the system. This can be implemented by cycling the dish on/off sun, or by actively cooling the PCM.

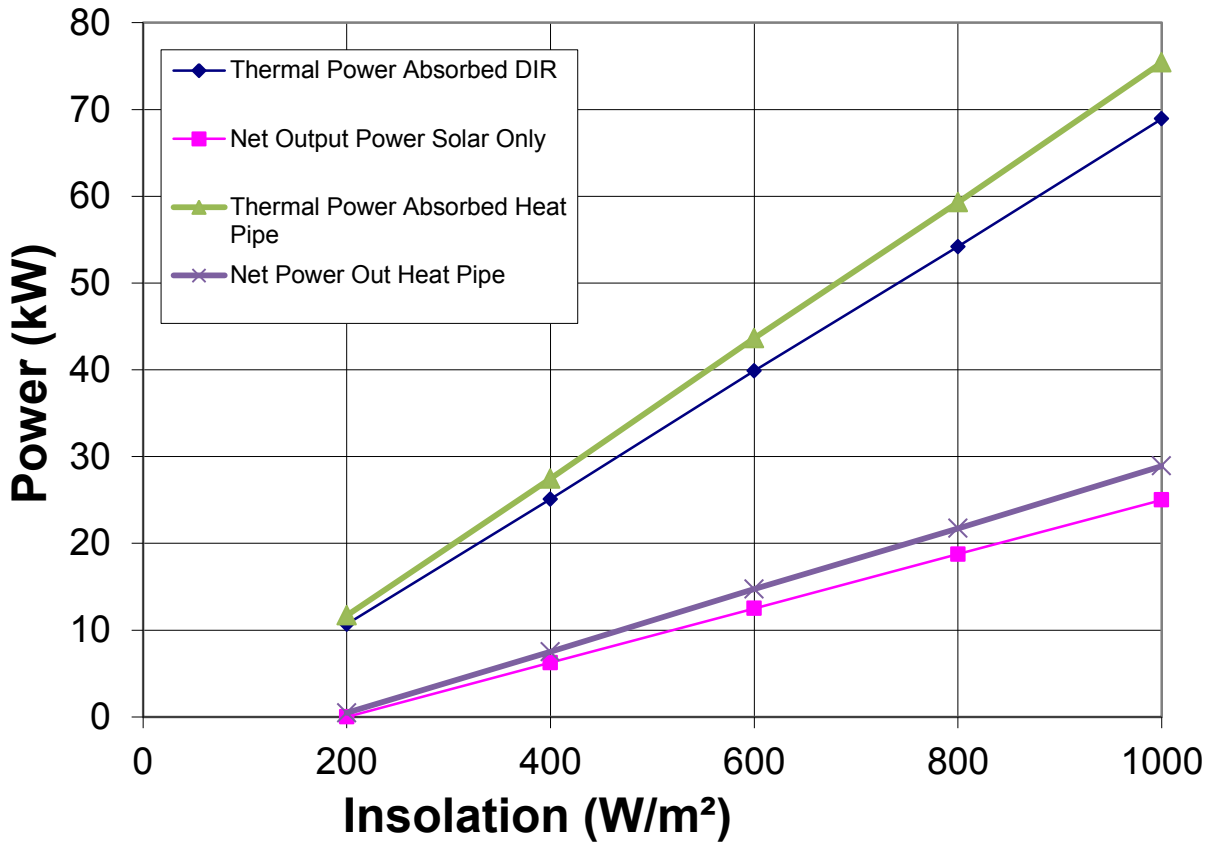

Figure 5. System and receiver performance. System performance based on measurements. Thermal performance extracted via receiver thermal models.

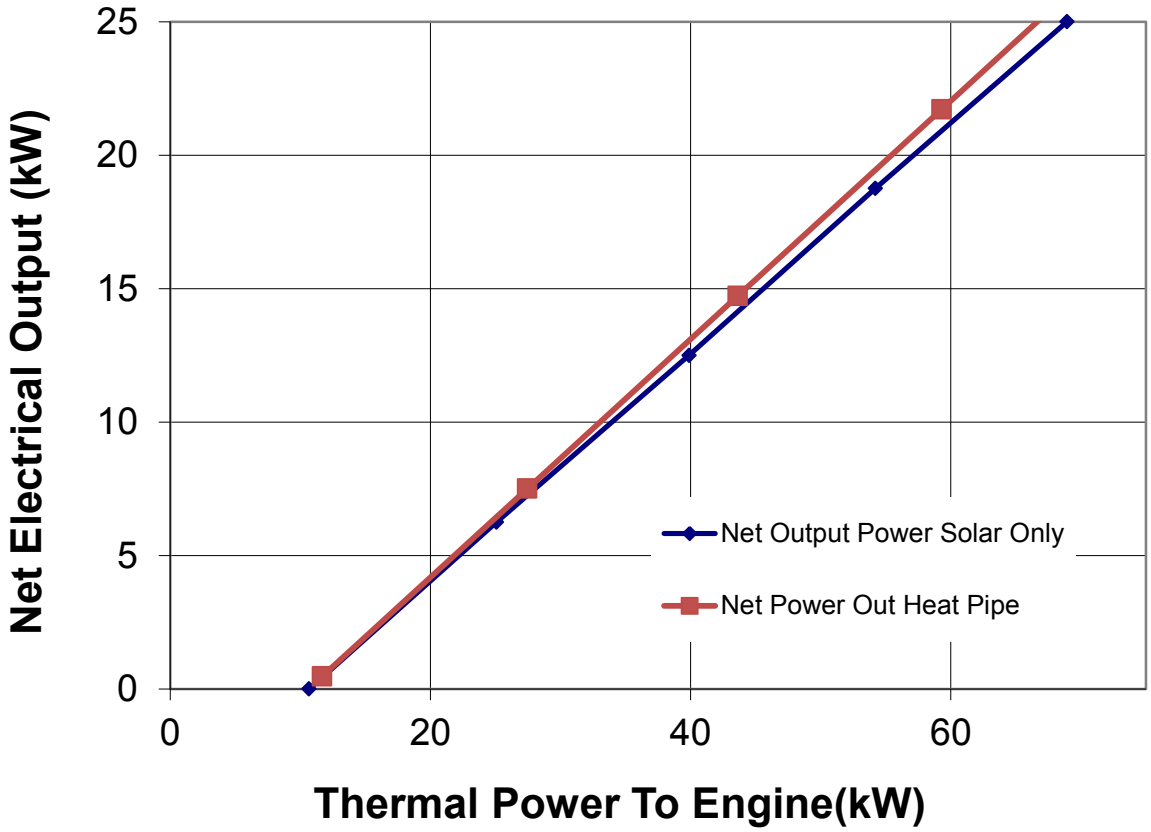

Figure 6. Engine performance based on the curves in Figure 5. The storage cases were run at 25kW engine output, absorbing 66.65kW$_t$ from storage.

Several parameters affect the storage system. The storage capacity is selected in kW-hr$_t$, or in hours of storage assuming full power operation of the engine during storage drawdown. The solar multiple could also be specified. This was simply a size scaling of the dish reflecting area, with a solar multiple of 1.0 equal to the original SES MPP-vintage dish. In reality, since the heat-pipe-driven system is more efficient, the baseline solar size should be reduced. In addition, the closing of the gap, touted as an advantage, is not accounted for in this systems study. It is assumed that the field size (dish spacing) will increase proportional to dish linear size, and therefore the shading as a percentage is still valid based on shading in the nominal field size.

Finally, a very simplistic financial model was included. The TOD —value" of the energy produced was calculated on the Southern Cal Edison (SCE) 2011 TOD periods outlined in Resolution E-4442 of the PUC of California, adopted December 1, 2011 [5], which provides the market price referent for California. The TOD table indicates multiplier factors for delivery at various times, which modify the base value of the electricity. I used a $0.10/kWhr base price, consistent with the market price referent for long-term (20-year) contracts in 2015. I did not escalate the payments, but rather modeled a single year of operation. I did not account for weekends or holidays, which currently have an alternative schedule. Table 1 shows the TOD multipliers for SCE for 2011.

Table 1. Southern Cal Edison TOD multiplier factors from 2011

Season	Period	Definition	Factor
Summer June 1 - September 30	On-Peak	WDxH[1], noon-6 pm	3.13
	Mid-Peak	WDxH, 8-noon, 6-11 pm	1.35
	Off-Peak	All other times	0.75
Winter October 1 - May 31	Mid-Peak	WDxH, 8 am-9 pm	1.00
	Off-Peak	WDxH, 6-8 am, 9 pm-midnight; WE/H[2] 6 am-midnight	0.83
	Super-Off-Peak	Midnight-6 am	0.61

1/ WDxH is defined as weekdays except holidays
2/ WE/H is defined as weekends and holidays

The revenue stream is generated by simply multiplying the energy generated during each 15-minute period by the price and the multiplier noted above. This revenue stream is summed for the entire field, and categorized by time of day and by month for analysis purposes.

A simplistic Levelized Cost of Energy (LCOE) is developed from the approach used by Sargent Lundy [4]. Equation 1 shows the calculation of LCOE for a simple system:

$$LCOE = \frac{\left(CC * FCR + OM_y\right) * RatedPower}{AE}$$

Where:

LCOE=Levelized Cost of Energy, $/kW-hr
CC = Capital Cost, $/W, set to $2/W
FCR = Fixed Charge Rate, set to 7.42%
OM_y = O&M costs in $/W/yr, set to $0.045/W/yr
Rated Power = Entire plant size in W, set to 500MW
AE = Annual Energy produced in kW-h, as calculated

The Capital costs were based on SES projections of their capital costs [1]. When storage was added to the system, the Capital Cost (CC) was modified to account for the cost of the storage system, in terms of the storage size (includes storage media and interface, both scale with size), a fixed charge for storage (includes the receiver, the vapor duct, the engine interface, and the sodium pump), and the solar multiple (scales the cost of the reflector system, including land, wiring, and other BOP aspects that scale with dish size. The modified CC calculation is then:

$$CCWS = \frac{(SFC + SVC * SC)}{RPPD} + CC * (1 - SF + SF * SM^{1.5})$$

Where

CCWS = Capital Cost With Storage, $/W
SFC = Storage Fixed Cost, $/dish, set to $3000/dish
SVC = Storage Variable Cost, $/kWh$_{th}$, set to $20/ kWh$_{th}$
SC = Storage Capacity, kWh$_{th}$, user setting
CC = Basic system Capital Cost, $/W, set to $2/W
SF = Scaled fraction of dish, set to 50%
SM = Solar multiple
RPPD = Rated Power Per Dish (W)

The first part of the equation represents the capital costs of the storage system itself. Then the capital cost of the system is modified to account for the larger dish. Only a portion of the system cost is scaled, as the engine, controls, and some other parts do not scale with solar multiple. The exponent of 1.5 on the solar multiple is based on Kolb's analysis of heliostat steel cost scaling with heliostat size [17].

The fixed storage cost per dish, at $3000, is an estimate of the eventual incremental cost of the storage system over the cost of the DIR system, and does not vary with the storage capacity. The $20/kW-hr of storage cost is based on an estimate of PCM cost if the PCM is a metallic such as Aluminum-Silicon, plus the incremental cost of heat exchangers, containment, and insulation that scale with capacity. These numbers can be changed as inputs by the user. In addition to the TOD value of the energy and the LCOE, profit is calculated as the difference between the two values.

3.3 Results

The model was exercised a number of times, varying the storage capacity, the solar multiple, and the start time of the engine output. The relative system performance is evaluated in terms of LCOE and profit. Secondarily, the shed thermal energy (when storage is full) is considered a significant system downgrade. If too much energy is shed, the value of the collection hardware is diminished. If no energy is shed, the storage media is probably oversized for the given solar multiple. Both these extremes of shedding impact the LCOE and profit.

The LCOE shows a clear minimum at a solar multiple of 1.25 (Figure 7). At higher solar multiples, the shed energy increases, and therefore the increased cost of the dish is not amortized over a proportionally greater amount of energy generated. The same trend is seen regardless of the storage capacity, represented by the various points at each solar multiple. The greatest impact on profit is solar multiple (Figure 8). The profit goes down with increasing solar multiple due to the shedding impact on LCOE, but also due to the lower value of the energy in the night hours. Collecting energy in the lucrative summer afternoon hours, but deferring electrical generation to the night hours has a negative impact on profit due to the TOD rate structure. Both the LCOE (Figure 9) and the profit (Figure 10) show little response to the hours of storage, especially in the cases of lower solar multiple (low LCOE or high profit). The spread in points at each storage capacity indicates the various solar multiples. Increasing storage capacity allows amortization of the system cost over more energy generated, but the system cost increases as well. As solar multiple increases, more energy is shed (Figure 11), meaning less electricity is generated and therefore less revenue. While a solar multiple of 1.0 is most profitable, the generation into the evening hours is limited, and the storage is rarely filled. A solar multiple of 1.25 allows significant evening generation, and typically only a few percent of total energy shed, and appears to be a good compromise. Figure 12 shows the shed energy re-arranged to compare to storage capacity. It is clear that, for a given solar multiple, there exists an optimal storage capacity, or vice versa.

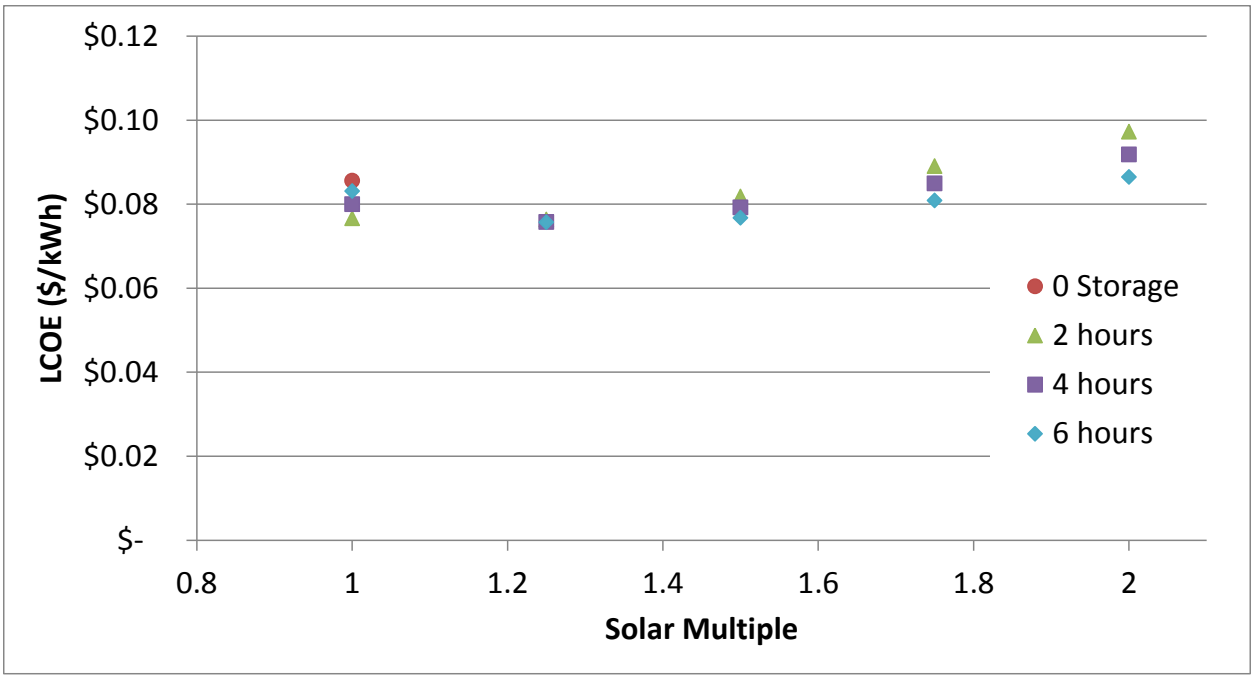

Figure 7. Impact of solar multiple on the LCOE. The red diamond is the non-storage DIR system. The different points at each solar multiple are for different storage capacities.

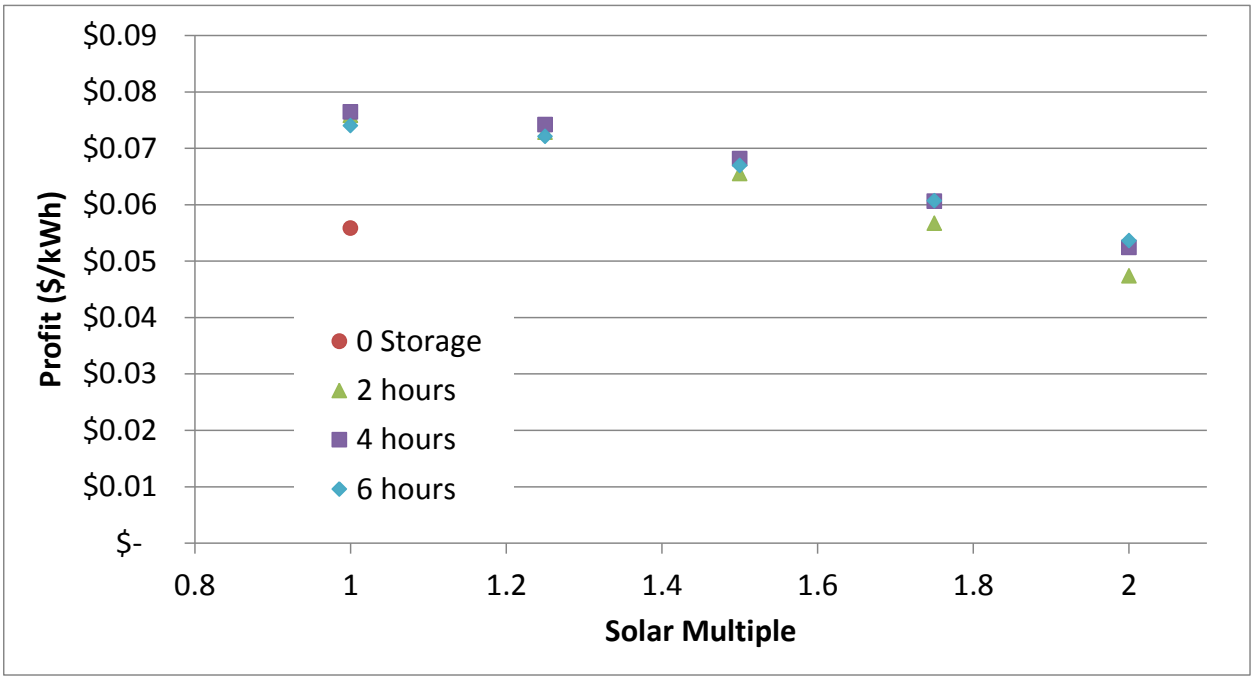

Figure 8. Impact of solar multiple on plant profit. Profit is the difference between the utility payment (based on a $0.10/kWh baseline) and the LCOE. The multiple points at each SM are for different storage capacities and start times

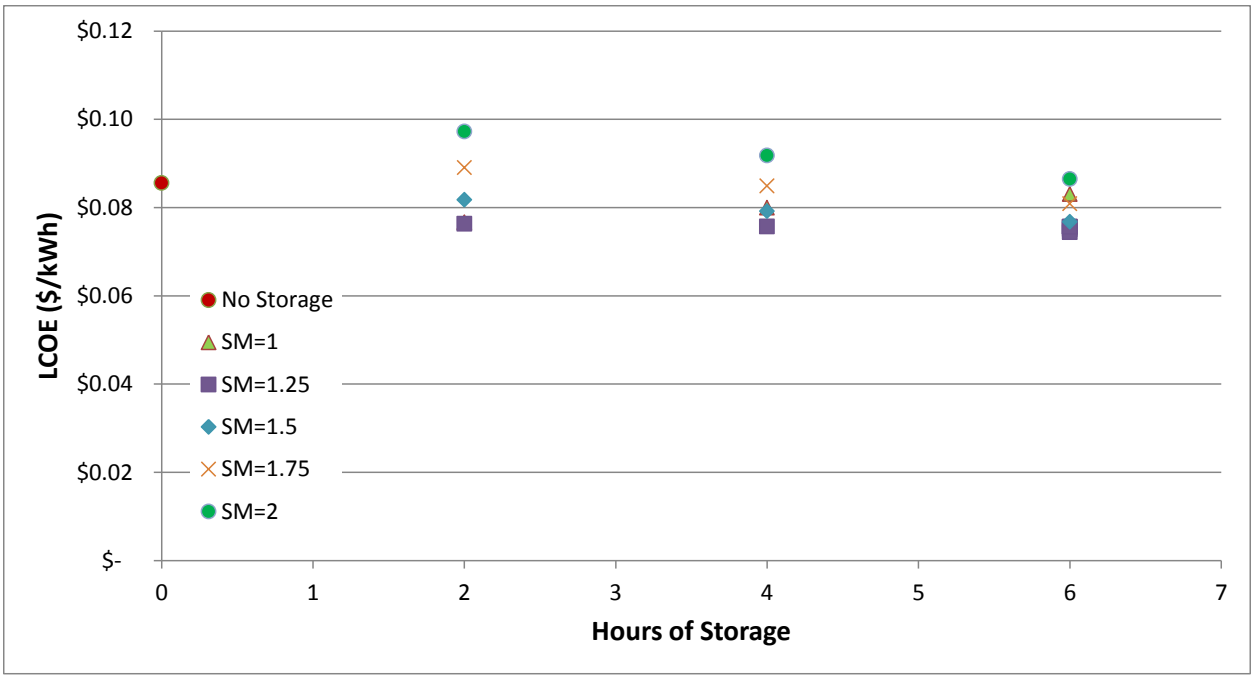

Figure 9. Impact of storage capacity on LCOE .

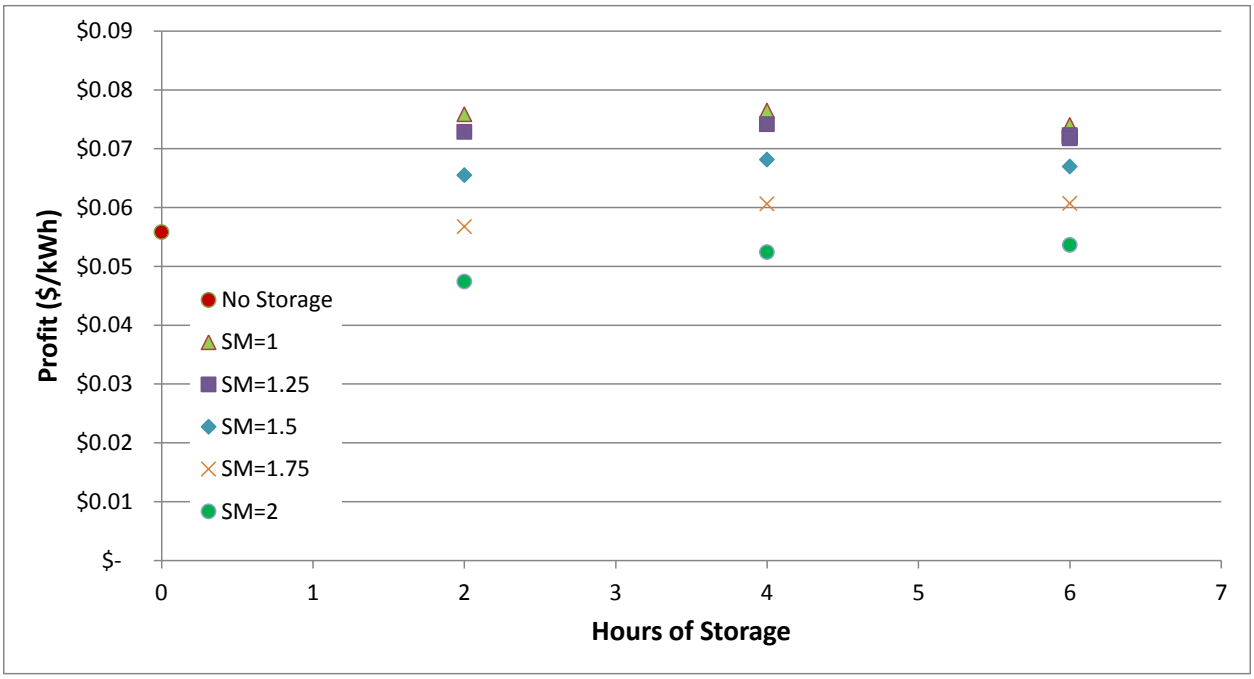

Figure 10. Impact of storage capacity on profit.

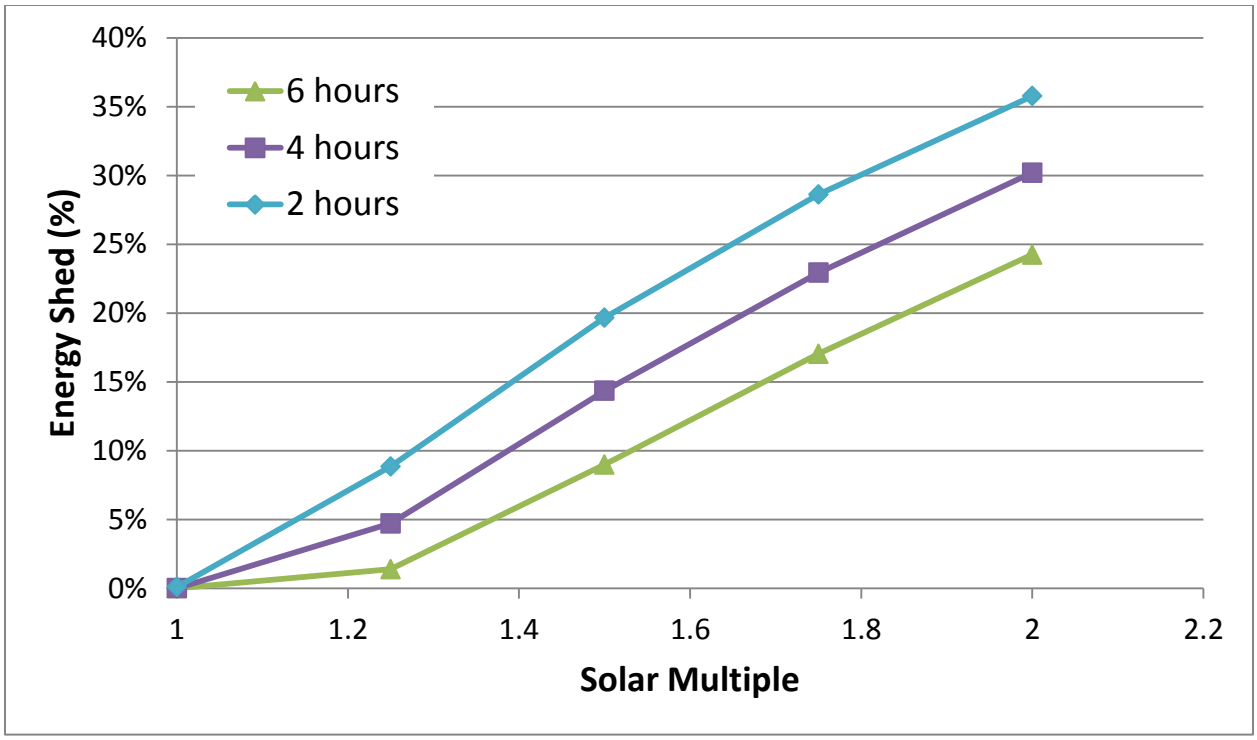

Figure 11. Thermal energy shed from storage due to storage capacity full while on sun, at different solar multiples and capacities (time of capacity).

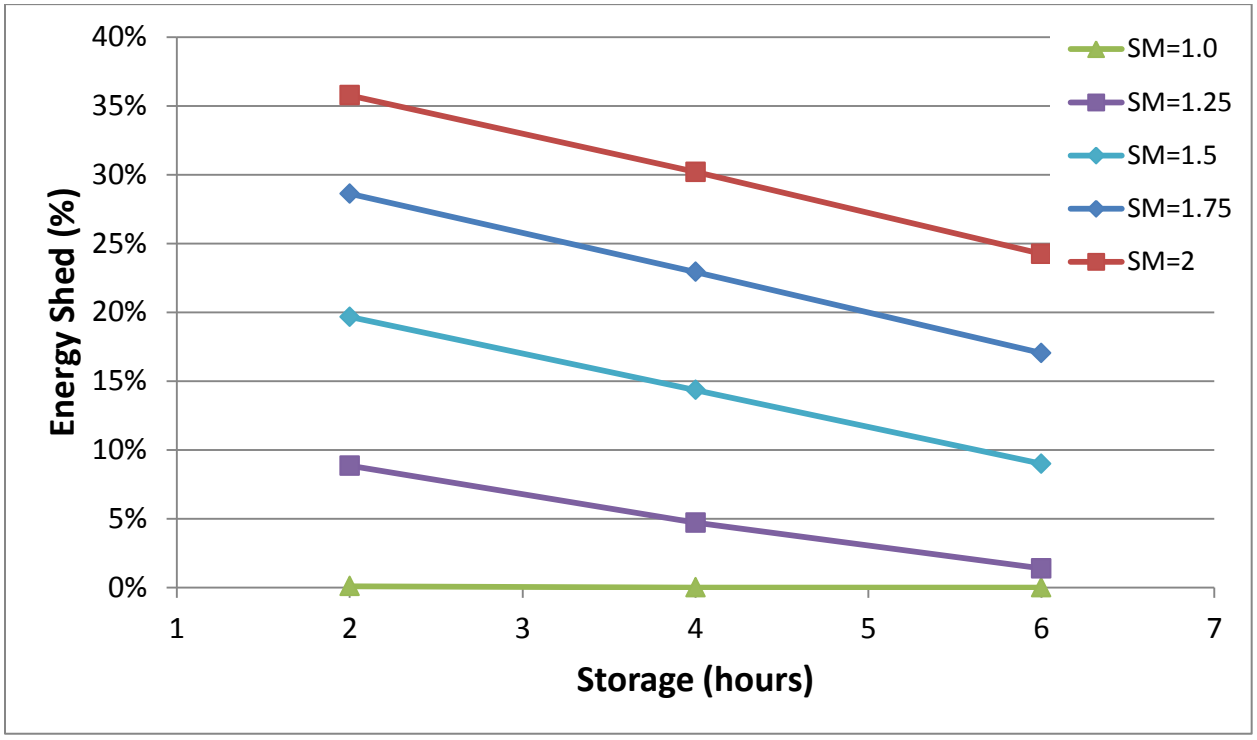

Figure 12. Shed energy vs. storage capacity

It is difficult to evaluate the efficacy of the storage system to extend generation into the evening, since the weather patterns vary throughout the year, as does the time of sunset. While the revenue predictions are helpful, they are based on current TOD patterns, which do not put a high value on storage. Figure 13 is an attempt to visualize the impact of storage on evening generation. I have plotted the stored thermal energy against elevation angle of the sun, for the afternoon hours only, for an entire year of TMY data. In this case, the solar multiple is 1.25, and the capacity is 6 hours of storage. If storage is full, then full engine power can be generated for 6 hours (in this case) after the solar input diminishes. It is clear in the figure that on most days the storage is full at 8-10 degrees solar elevation. Storage starts to deplete at this point due to reduced solar input as well as in-field shading. While there are some days with less than full storage, and some with no energy stored at all, the majority of days have relatively full storage at the end of the day. Figure 14 shows similar data with the solar multiple set to 2.0. While fewer days have partial capacity (the middle of the graph is less congested), the impact is limited, and the maximum capacity is not increased. Of note is that there are still many days with little or no storage filled at the end of the day.

The systems model also reports the monthly energy generated by hour of day, which gives insight into evening hour generation, Figure 15. This data is from the case of 6 hours of storage and 1.25 solar multiple. During the summer months, significant energy is generated through midnight, whereas in the winter, little energy is generated past 9pm. Figure 16 shows the case without storage. The summer evening power only extends into the 6pm hour without the benefit of storage. Figure 17 shows the same data with storage, transformed into a revenue stream, indicating the extreme importance of operation during the summer peak times as defined by the TOD tables. The summer afternoon energy and revenue are maximized with the storage system. Figure 18 shows the revenue stream without storage. Without storage, the system does not take full advantage of the lucrative summer afternoon hours.

All of the reported cases are run with a fixed incremental cost of storage of $3000 per dish, and a variable storage cost of $20/kWh$_{th}$. In the preferred case, 6 hours of storage and a solar multiple of 1.25, both the profit and the LCOE are significantly improved over the base case of no storage. In this case, the total cost of the storage system is $21k per dish, or $52/kWh$_{th}$. The LCOE is $0.076/kWh$_e$, compared to the non-storage case at $0.086/kWh$_e$. The profit is $0.072/kWh$_e$ compared to $0.056/kWh$_e$ without storage. This benefit demonstrates that the proportions of system cost proposed in the SunShot initiative, which requires storage at $16/kWh$_{th}$, is not developed for dish Stirling systems. Further, if we adjust the cost until the LCOE is unchanged with storage compared to the non-storage case, we find the total storage cost can be $33k/dish, or $82/kWh$_{th}$, a substantial difference from the tower case in the SunShot initiative. This finding indicates that one can pay a substantial cost for storage and still see a system improvement. The allowable cost for storage is even greater if profit, not LCOE, is considered. This difference when compared to towers is likely primarily due to the very high electrical generation efficiency of the Stirling cycle engine, and high exergy efficiency of the proposed system.

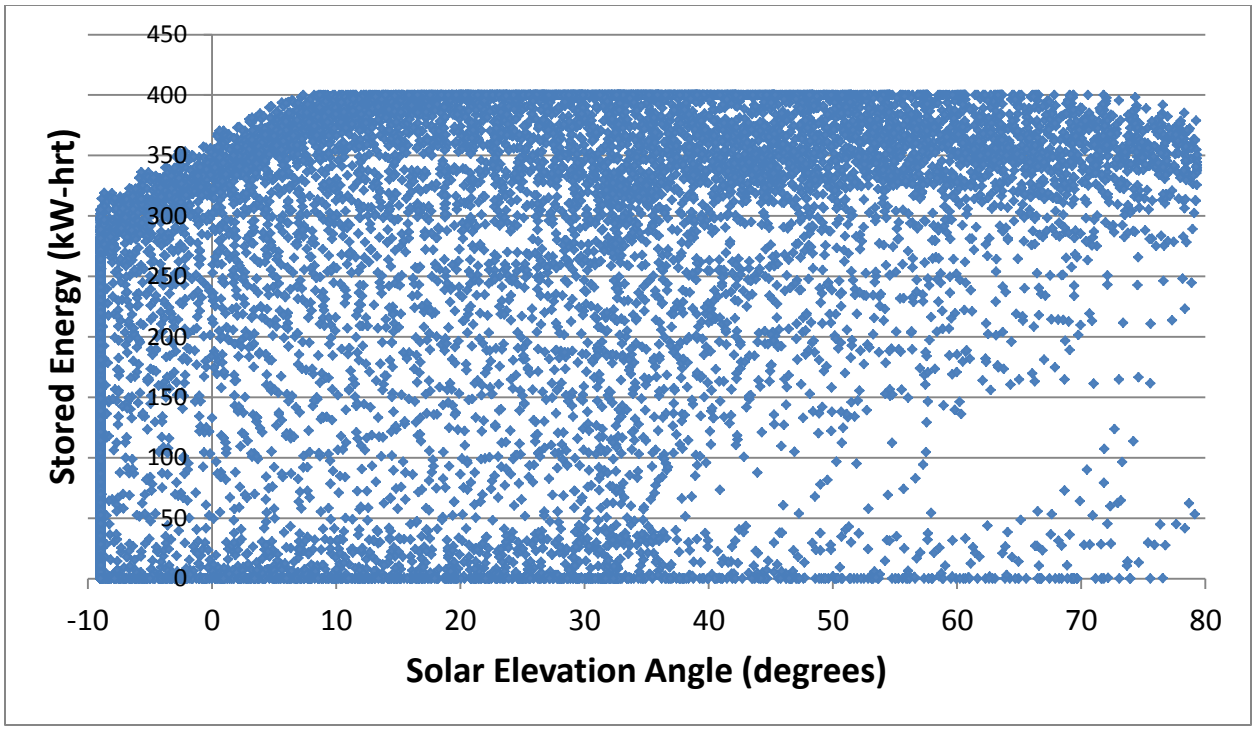

Figure 13. This scatter plot shows the amount of energy in storage in the afternoon, relative to solar elevation angle (as the sun goes down).

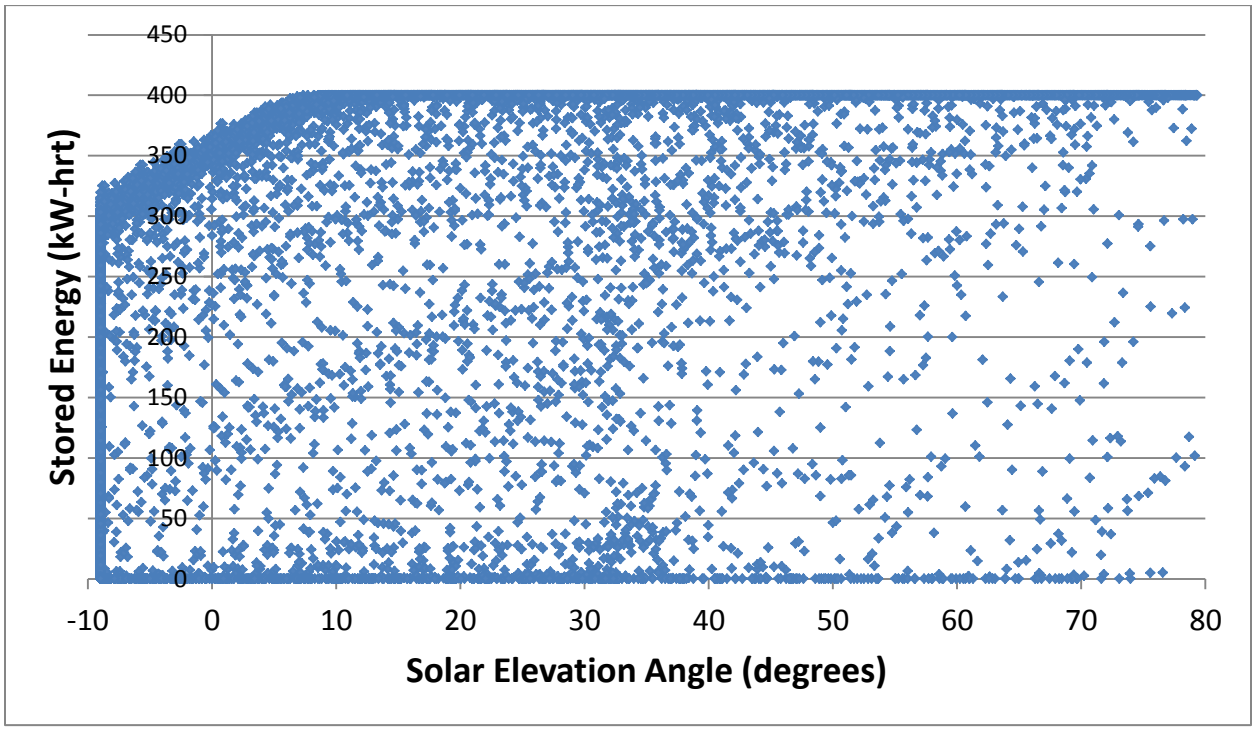

Figure 14. Afternoon storage utilization with Solar Multiple 2.0

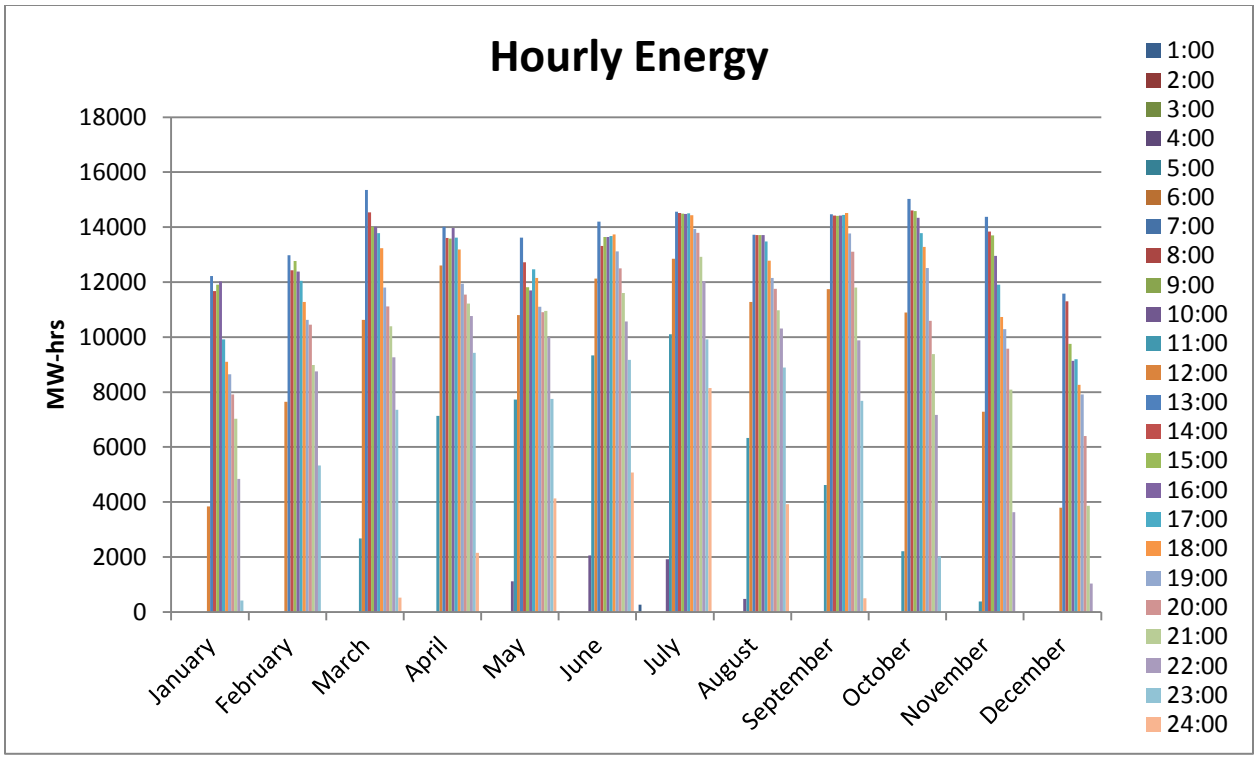

Figure 15. Hourly energy produced per month with storage. In the summer months, significant energy is generated to the midnight hour.

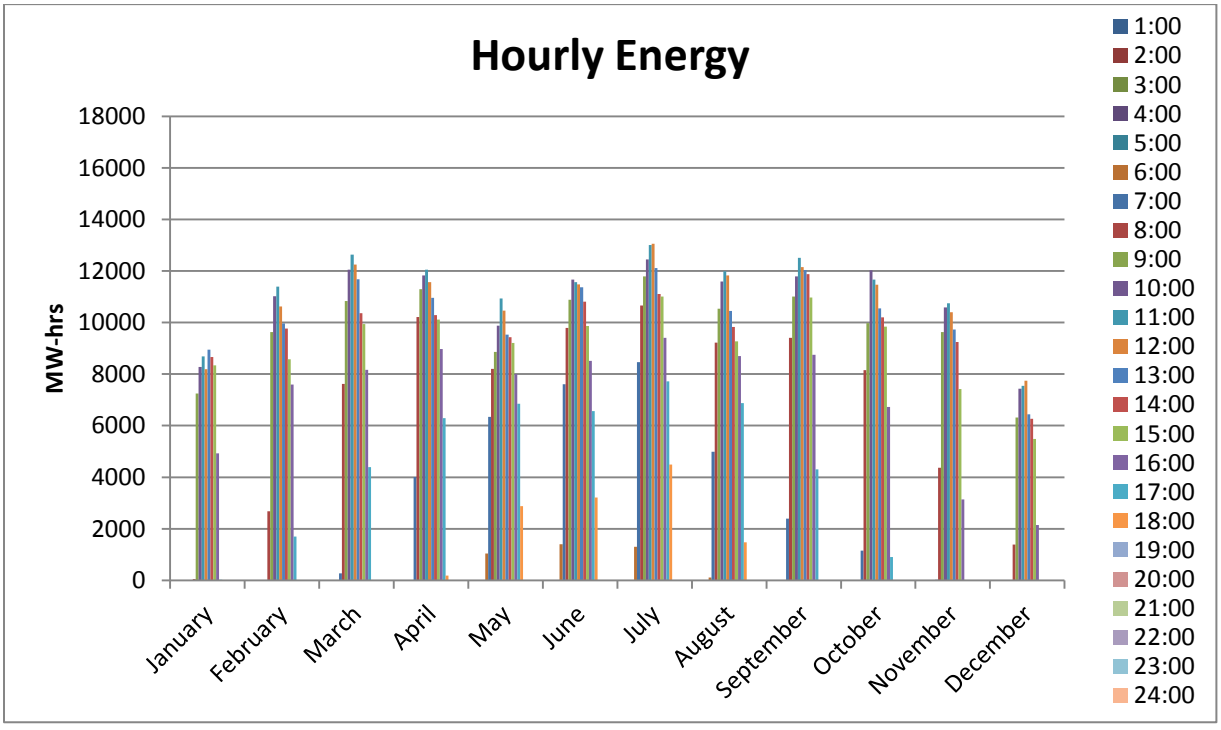

Figure 16. Hourly energy produced per month without storage. In the summer, the latest energy produced is in the hour starting at 6pm.

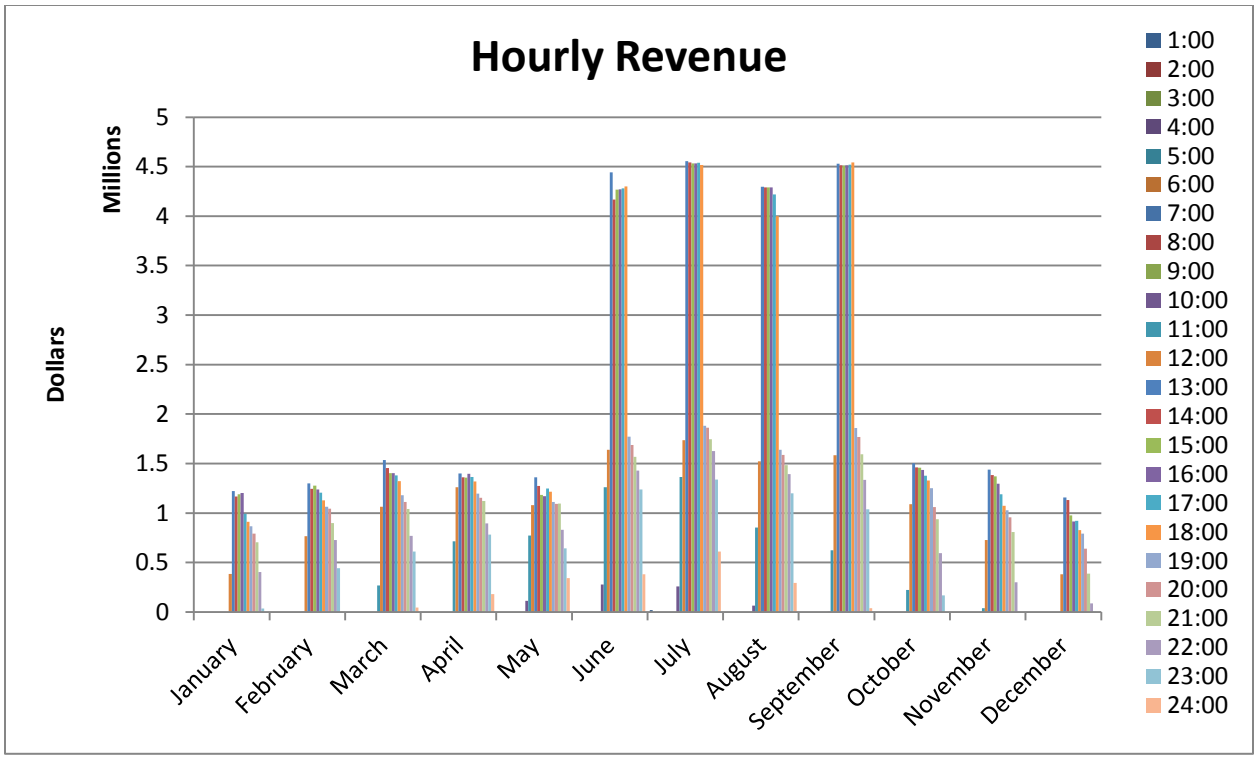

Figure 17. Hourly revenue produced by month with 6 hours storage and SM=1.25. Notice the extreme importance of the summer afternoons to the overall revenue stream.

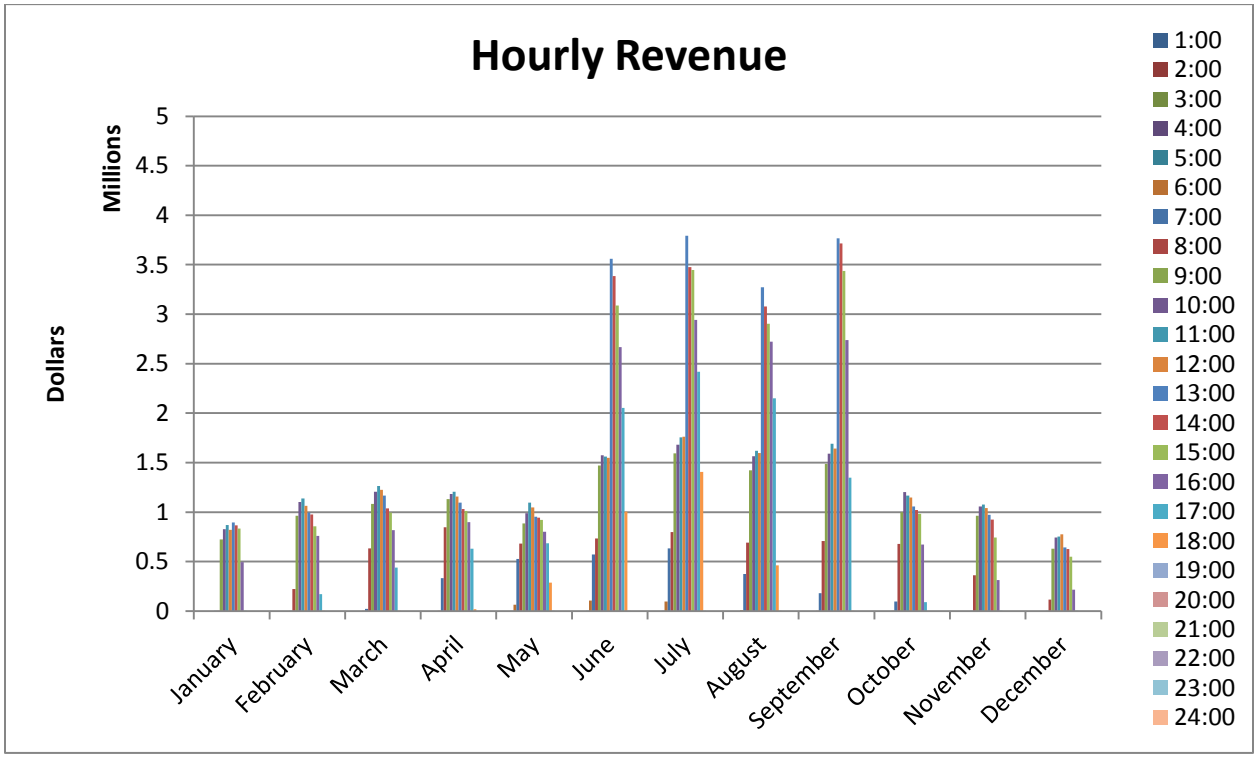

Figure 18. hourly revenue produced by month, without storage.

3.4 System Model Conclusions

Based on the limited modeling performed, it does appear that storage can improve the LCOE of a dish-Stirling system, despite adding to the cost of the system. This is because of several impacts:

1. The receiver and engine performance are enhanced by the heat pipe receiver and heat pipe transfer to the engine, as demonstrated in earlier non-storage heat pipe work.
2. The engine runs at rated power whenever it does run, which improves the overall annual efficiency. The engine is never run above the rated power, an important life consideration not included in the LCOE calculation.
3. The engine runs at full power during most of the summer afternoon peak, shifting some morning collection into the lucrative afternoon generation period
4. The storage system allows amortization of system costs over a greater amount of annual energy generation

The impact on profit, determined by the TOD factors of SCE, is even greater than the impact on LCOE. Further, the storage system can cost as much as $\$82/kWh_{th}$ without negative impact on the LCOE, or \$33k/dish over the solar-only option.

It appears that the solar multiple does not have to be substantive, and in fact too high a solar multiple relative to the storage capacity leads to excessive thermal energy shedding, reducing the efficacy of the expensive collector system. My observation is that a solar multiple of 1.25 is sufficient to fill the storage on most days, and limits shedding to under 5% of the total energy. This puts the dish size on the order of 100 m², and the heat pipe receiver thermal input to about 94kW, which is within the realm of possible solutions with a Sandia high performance wick structure. This solar multiple also minimizes LCOE, and has minimal impact on profit, compared to the SM=1.0 case.

The duration of storage required for optimum performance form a profit standpoint will depend upon the TOD revenue tables. With current TOD tables, the evening hours are not as highly valued as daytime hours, and therefore the size of the storage may be driven smaller. However, if we assume the PUC‘s and utilities will put further value on evening generation, then it appears that 6 hours of storage, the highest level considered, should be pursued. This allows summer operation on most days past 11pm. As evening value is increased, the optimum hours of storage may also increase. However, it is unlikely that more than 6 hours of storage on a dish system will be technically desirable, due to mass and size of the storage system and the throughput requirements of the receiver heat pipe wick with higher solar multiple.

Higher solar multiples and higher storage capacities do not help on days in which little to no energy is collected. Since these days do exist, a backup generation system must be considered at the utility level, whether on site or a part of the whole grid environment. It is not economically feasible to size the system for multiple days of sunless operation, when the vast majority of the days can generate energy in the currently considered configurations. As with all solar systems with storage, high capacity cannot be practically guaranteed, and some backup, either on site or on the grid, must be used for cloudy days and extended outages. Sufficient storage to cover extended cloudy spells is simply not feasible, as the utilization of the extended capacity, and utilization of the increased capital cost, will be minimal.

Alternative controls strategies can be considered, which can extend operation to later hours by foregoing generation, or reducing power output, during the daytime. This may be a reasonable path in the winter, if the evening home heating load is significantly electric. However, in the summer, the system usually started generation before noon, triggered by full storage. A larger storage capacity could allow later starts, but may be under-utilized on an annual basis.

The economic details of a particular project, namely the TOD revenue stream and any capacity payments or penalties (not considered here), must be considered when sizing storage or the solar multiple. In addition, the PUC or transmission company may impose further requirements on the operating scenario that are not considered here. For example, significant penalties may be imposed for not generating at key times, or not predicting generation accurately in advance. The storage system, even at a fairly small capacity, can provide a buffer for response times to unexpected poor or transient solar conditions, allowing the utility to bring other reserves on line with sufficient notice, and avoid penalties. The costs and other economic considerations in this high-level look should be considered parametric, rather than representative of a particular installation.

4 EXERGETIC ANALYSIS

We performed a preliminary exergetic loss calculation to determine the feasibility of this system meeting the ARPA-E goal of 95% exergetic efficiency. Because the thermal losses scale with the square of dimension, and storage scales with the cube, it is unlikely that the *laboratory subscale prototype*, at up to 30 kW_{th} storage, will meet this requirement. In the following exergy analysis, we consider a 80 kW_{th} system with 6 hours of storage, or 480 kWh input over a period of 6 hours of charging operation. This represents a feasible embodiment for a 25 kW_e dish-Stirling system, and should meet the storage efficiency requirements.

The ARPA-e FOA call defined exergetic efficiency as

$$\varepsilon = \left|\frac{\Delta G_d}{\Delta G_c}\right| = \left|\frac{(\Delta H - T_{amb}\Delta s)_d}{(\Delta H - T_{amb}\Delta s)_c}\right| = \left|\frac{W_d}{W_c}\right|$$

where the subscripts c and d are for the charging condition and the discharging condition respectively. For a purely thermal system, this can be re-written such that

$$W = Q\left(1 - \frac{T_{amb}}{T}\right)$$

for each condition (charge and discharge), where W is work, Q is heat transferred, T is the available temperature, and T_{amb} is the ambient temperature, defined as 298 K for the proposal. We further define

$$Q_d = Q_c - \sum Q_{loss} \qquad T_d = T_c - \sum T_{loss} \ .$$

If we consider a control volume around the storage container only (Figure 19, CV 3), we can determine the exergetic efficiency of the storage media and containment. For this we use the temperature in the sodium vapor just upstream of the storage, and again downstream of the storage. The temperature drop is defined by thermal transport through the heat exchanger and PCM. Q_{loss} for this scenario is due to conduction to the environment over a 12-hour period (6 hours of charging and 6 hours of discharge). We assume a PCM of NaCl, with a melting point at 801 °C and a total volume of 1.65 m^3, in a spherical containment with 1 foot of aerogel insulation. The energy lost in this point example is 6.2 kWh. We consider a range of temperature drop across the PCM system, and calculate the resulting exergetic efficiency, shown in Figure 20. This indicates that the maximum allowable temperature drop across the PCM is about 45 °C, which is tunable by optimizing the area of the heat exchanger contact with the PCM. The thermal transport across the PCM may be by conduction, convection, or a combination, and is only considered parametrically in this simplified analysis.

After the ARPA-e concept proposal, we were asked to consider exergy losses in the transport system as well as the storage system (Figure 19, CV 2). Based on an 80 kW_t heat input to the receiver and an 800 °C receiver vapor temperature, the mass flow rate of Na required to carry this energy from the receiver to the thermal energy storage system is 21.7 g/s (for a latent heat of vaporization of 3967 kJ/kg at the saturation temperature). This mass flow rate results in a mean velocity of 20.9 m/s and turbulent flow in a conservatively sized 4-inch diameter tube. For a transport distance of 8 m (on a 6.5 m focal length dish), the pressure drop at this mass flow rate is approximately 45 Pa, following

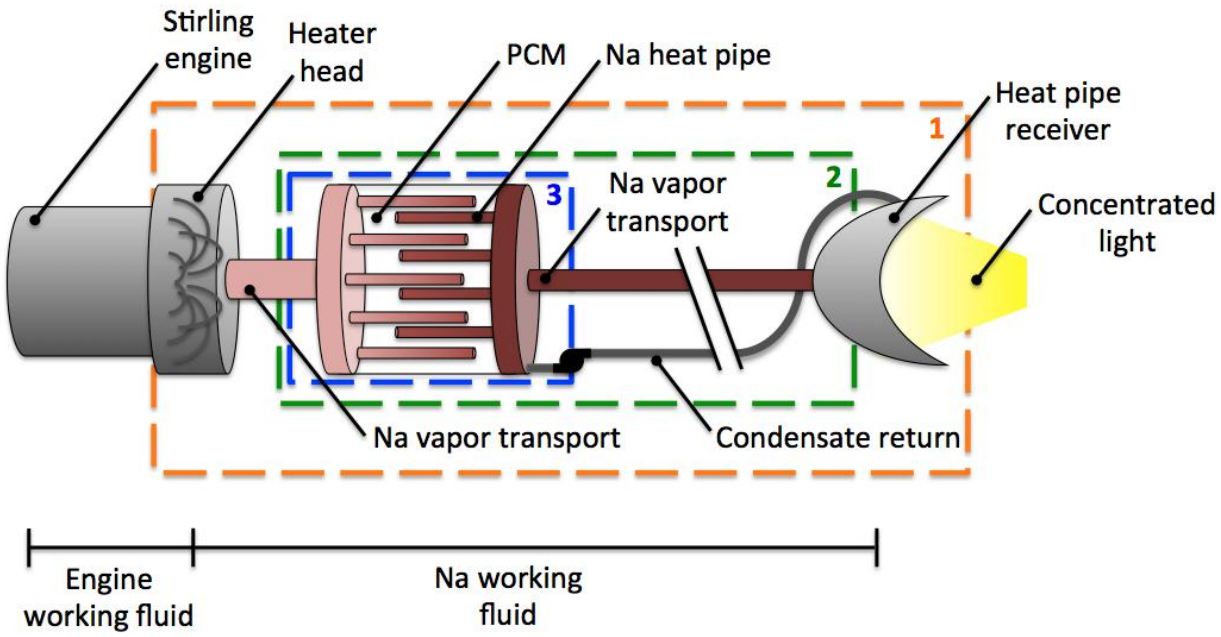

Figure 19. Schematic of dish-Stirling storage system, showing the various control volumes considered in this analysis

$$\Delta P = f \frac{\rho_{vapor} v_{mean}^2}{2D} \int_{x_1}^{x_2} dx.$$

Because the saturation pressure at 800 °C is 45.3 kPa, the pressure drop associated with the movement of the Na vapor would result in a well less than 1 °C decrease in saturation temperature during the transport from the receiver to the thermal energy storage system making the second law loss due to temperature decrease over this length minimal. The engine is closely coupled to the PCM containment in contemplated configurations, so likewise little temperature drop is expected. The heat loss (first law) can be easily estimated for an insulated pipe at constant temperature; for 6 hours (charging only) at 800 °C, about 2.54 kW_{th} is lost. By extending the exergy control volume for the thermal energy storage system to include the transport lengths, the exergetic efficiency reduction is minimal as shown in Figure 20. A 95% exergetic efficiency is expected for even large temperature differences (~45 °C) across the thermal energy storage system similar to the exergetic efficiency for the thermal energy storage system alone. The decrease in exergetic efficiency with the inclusion of the transport legs is on the order of 0.5%. PCM system multiphase heat transport modeling will be used to optimize the ΔT vs. cost.

We can further see the impact of the heat pipe/PCM storage system on the entire dish-storage-engine system exergy efficiency if we expand the control volume to include the conversion of concentrated sunlight to thermal energy, and the transfer of heat into the engine working gas. While this exergy efficiency is beyond the scope of the ARPA-E call, we see substantial improvements in this area, which lead to higher overall system performance, and can offset costs or losses introduced by the storage system. For this study, consider a control volume that includes all components from the receiver aperture (power through the hole and temperature on the receiver surface) to the engine working gas (temperature and power in the engine cycle) (Figure 19, CV 1) for two configurations:

- First, as a baseline, a DIR and no storage mechanism comprised a receiver and engine heater head where the working gas flows directly through tubes in the receiver to pick up thermal energy incident on the tubes and returns to the engine.
- Second, following this proposal, consider a control volume with heat pipe receiver, saturated vapor transport to a PCM thermal energy storage unit, a second leg of vapor transport to the engine heater head where the engine working gas is heated.

These cases encompass exergy drops beyond the storage and transport system, but provide a common boundary that can be used to compare the DIR system with the heat pipe storage system. Measured data reported in [8] is used to support the temperatures and efficiencies in this analysis. For an engine working gas temperature of 680 °C, the DIR has a front surface temperature of about 900 °C. The DIR cavity first-law performance was measured and analyzed at 85%. Thus, for 86 kW_{th} of concentrated sunlight through the aperture, 73 kW_{th} is delivered to the working gas in the engine cycle. For the heat-pipe storage system, we again assumed the PCM operates at 801 °C, and used the thermal losses noted above. Prior testing has shown that the air surface of the heat-pipe receiver is approximately 30 °C above the local sodium vapor temperature. Testing has also indicated that the engine working gas temperature is 116 °C below the local sodium vapor temperature. The heat-pipe receiver cavity was measured at 93% first law efficiency. 80 kW_{th} is delivered to the sodium vapor at the receiver, matching the earlier analysis.

Although there is the addition of transport lengths and a thermal energy storage unit, the proposed system exhibits a total exergetic efficiency of 75%–79% whereas a simple DIR system has been shown to be

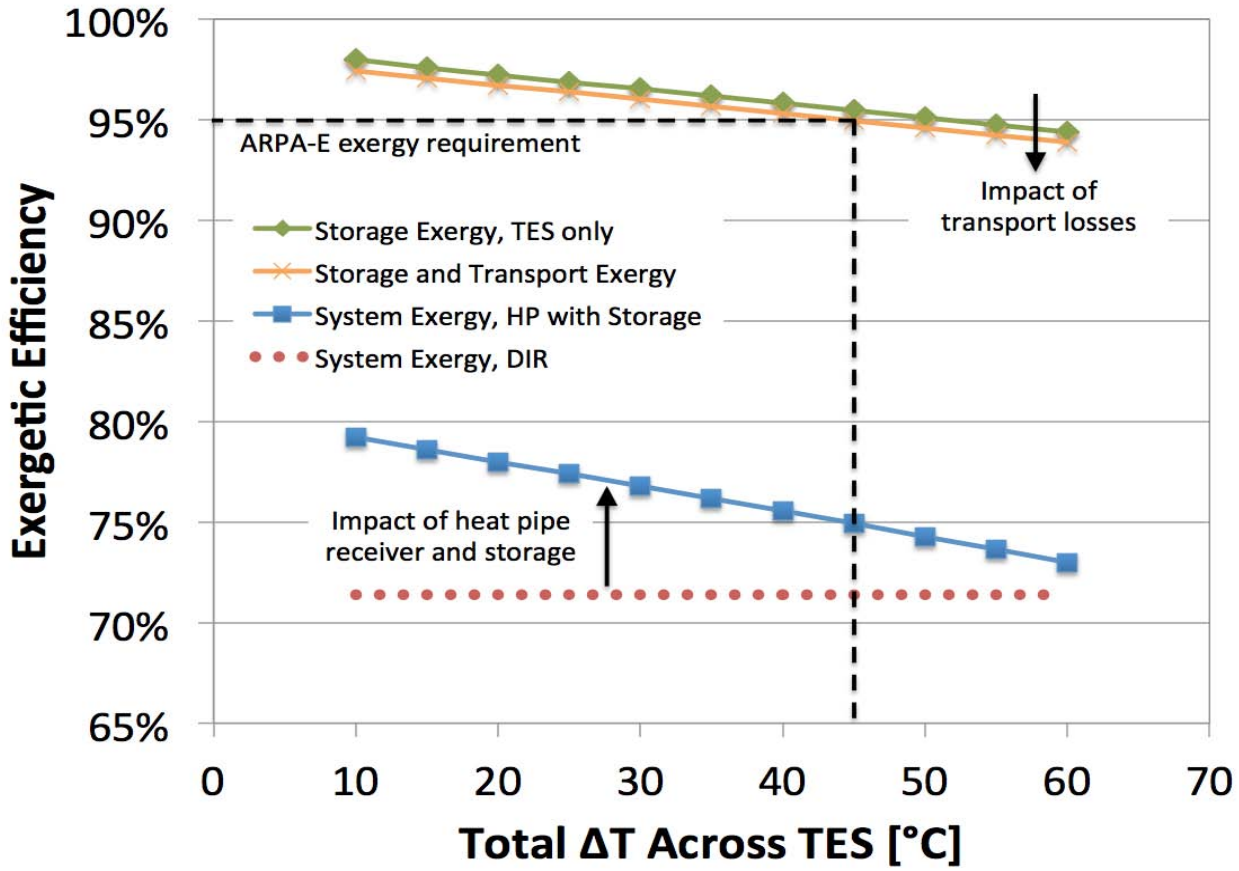

Figure 20. Exergetic efficiency comparison for the heat -pipe storage system, and for the entire heat conversion system for both the current DIR and the heat -pipe storage system.

about 71.4% (Figure 20). The first law losses in the DIR, as well as the higher air-side temperature, lead to this poorer exergetic performance of the DIR system. By moving to a heat-pipe receiver, thermal energy storage can be added to a dish-Stirling system while still maintaining an exergetic efficiency above that of current technologies. This is a transformative approach to harnessing the concentrated energy in dish-Stirling systems and enables thermal energy storage without penalty to the full system.

5 HEAT PIPE CONFIGURATION

5.1 Requirements

The heat pipe system for a solar receiver presents a unique set of challenges not seen in many heat pipe applications. The heat pipe must transfer large quantities of heat (60 to 100 kW) at relatively high input flux levels (100W/cm²) at high temperatures (800°C), over a large areal extent. Typical heat pipes in the literature are tubular, with internal (concave) wicks, whereas the solar interface is on a dome with a convex wick structure. The startup of the heat pipe is rapid (seconds to minutes) compared to typical high temperature heat pipe systems. The high power combined with high flux puts stringent requirements on the pumping capability of the wicks, both locally and globally. Table 2 presents the high-level specifications for the receiver heat pipe. The evaporator for the engine interface will be more conventional tubular pipes, with gravity-assisted return (thermosyphon).

The heat pipe system must operate in the atmosphere, and therefore must withstand air-side corrosion at high temperatures. Initially, Haynes 230 alloy is selected as a robust containment with good corrosion resistance. However, for lower cost, stainless options with passivation coating should be considered.

Table 2. High level heat pipe receiver specifications

Parameter	Target value
Thermal throughput	80-100kW$_t$
Temperature	800°C
Working fluid	Sodium
Physical size	18” diameter dome, 70° half sphere angle
Gravity	0 to 90 degrees during operation
Peak flux	75 W/cm²
Average flux	~35 W/cm²
Startup	Self priming, no arteries
Life	20 years
Environment	Air, moisture
Liquid distribution	EM pump or gravity return, wick distribution

5.2 Wick Technologies

The wick system for distribution of the working fluid across the heated dome is a critical area, and requires demonstration of capabilities to transport sufficient power at sufficient flux, while remaining stable for sufficient duration. The requirements above are stringent for conventional heat pipe wick technologies. A number of commercial and developmental wick approaches have been considered and are outlined below.

Two US companies work with high temperature heat pipe systems commercially, Thermacore Inc. and ACT, both in Pennsylvania. ACT was formed by several prior Thermacore high temperature heat pipe experts. Both companies use sintered powder wick systems, usually with arterial structures, which have proven effective in low temperature systems for electronics cooling. Very good performance is achieved through a pore radius distribution that allows the generation of vapor within the wick while still transporting liquid transversely. Performance is typically enhanced with arterial structures, either with protected straw-like arteries [18] or large sintered structures [19] with lateral transport from a closely-coupled condenser sponge. Shaubach et. al. [18] demonstrated 5.4kW throughput at fluxes to 50W/cm² in

an axial heat pipe. Hwang et. Al [19] demonstrated an extremely high flux of 580W/cm² over a 1cm² heater area using water, for high-power electronics cooling. This application demonstrates the tradeoff between power (areal extent) and peak fluxes, and shows that an extensive artery structure can feed a small area with sufficient fluid for high flux performance. The sintered powder systems, while out-performing groves and screens due to the ability to accommodate vapor generation in the wick, fall short of the performance requirements of solar receivers, and have been shown to lack robustness when installed on a large dome that must transition through a large temperature range. The sintered structure is somewhat brittle, and struggles to accommodate the surface shape changes with non-uniform rapid startup heating [20]. The sintered structure, however, is the commercial state-of-the-art for both high and low temperature, high performance heat pipes.

A Bi-disperse wick structure [21] has been proposed and tested for high flux wicks that allow vapor generation in the wick. The concept has a sintered structure of particles, which themselves are sintered from many smaller particles. This structure allows vapor passage between the larger clusters while allowing liquid communication along the surfaces of the smaller particles. The structure is complex, and the liquid path tortuous and limiting. The sintered structures by Thermacore and ACT, as well as Sandia's felt wick structures have poly-disperse pore radii, allowing similar enhancement through tailored pore distributions, rather than two discrete pore radii.

Most recent heat pipe efforts focus on high flux electronics cooling, where the peak fluxes are anywhere from 100 to 500 W/cm², but the total power and areal extents are small. The sintered powder efforts noted above in [19] are an example of the sintered powder approach. Microgroove heat pipes with water, alcohol, or ammonia working fluids have been studied extensively, but are limited to low-temperature applications with low total power extraction [22]. Zuo et. al. [23] reports on a unique approach to electronics cooling using a "pulsed heat pipe". This is a close-coupled evaporator and condenser, with multiple transport tubes and an over-fill of the working fluid. The excess fluid is alternately entrained in resonant flow between the ends of the system, enhancing heat transfer to 200W/cm² in tuned systems for electronic cooling. The geometry required to establish resonance is not compatible with the necessary distance in the proposed system.

Loop heat pipes [24] address entrainment issues in counter-flow heat pipes for transmission of heat over long ranges, where entrainment is more limiting than wick issues. Loop heat pipes have received attention for electronics cooling as well as reactor cooling where separation between the evaporator and condenser is required. The cited example reached total powers of 900W with low fluxes under 6W/cm² with sintered powder wicks containing vapor removal channels. The intent of loop heat pipes is to address the entrainment, but do not address the power and flux requirements (wick limitations) of the solar interface.

High temperature heat pipes typically contain sodium or other alkali metals for the working fluid. Considerable attention has been spent on corrosion issues in such heat pipes. Sandia performed significant work on resolving sodium-side corrosion issues [25], and developed cleaning methods that have been successful in avoiding corrosion of stainless steel fine wick structures and stainless or Haynes-230 alloy containment. These approaches have been used by Thermacore and ACT in successful long duration heat pipes [26] with some samples approaching 100,000 hours of operation without failure. Similar approaches to heat pipe processing have been documented recently by NASA [27] and incorporated by Infinia in their FOA work for DOE. Air-side corrosion of cost-effective containment materials has also been an issue. Sandia and Thermacore, under DOE programs, settled on Haynes-230 alloy as a sodium-compatible containment that could resist oxidation at 800°C in air. Merrigan et. al. [28] considered ceramic protective coating for higher temperature systems using refractory metals for containment. However, at this point, these coatings are not as cost-effective as Haynes alloy.

Prior DOE-funded heat pipe development at Sandia led to felt-metal wicks that were demonstrated to have sufficient performance for the proposed application, but lacked robustness. Like sintered powder, these wicks allow vapor generation within the wick, enhancing performance. The sintered felt structure contains a range of pore sizes, allowing vapor within the wick without drying the wick out [10]. The substantially higher permeability and porosity compared to sintered powder lead to higher performance. The small fiber diameters led to collapse of the wick over time at temperature. The weight of the supported sodium column compress the wick over time (creep), and with reduced surface permeability, eventually the vapor generation can cause surface damage to the wick.

Baturkin et al [29], under contract to DOE's IPP program, developed sintered felt wicks using a larger fiber, with vapor vent features, that addressed the key durability issues. However, some performance was lost due to the larger fibers used. The single sample tested at Sandia [30] indicated marginal performance, though it still out-performed nickel powder wicks. Recent modeling indicates that a thicker version of the same wick, or potentially a graded wick, could provide the robustness combined with sufficient performance.

The demanding performance and durability requirements of the heat pipe solar receiver can be met with the felt metal wick structures previously developed at Sandia. The robust versions of the wicks developed under the IPP program need to be demonstrated under long-term durability testing under conditions that simulate full-scale operation, and which can be used to validate models. In addition, some of the lost performance must be recovered while not compromising the durability of the wicks. The high performance wick is a critical element of the dish storage system. The proposed work is a durability test of previously-developed technology, and not a development of an entirely new wick. The proposed work will leverage the experience with the Baturkin robust, relatively high performance wick to demonstrate a wick with sufficient operational margin at high throughput power as well as sufficient strength for the life needed in a solar plant. This wick technology has not been matched by present industry or scientific efforts in meeting the requirements for high flux, high power, large areal extent, high temperature operation for extended periods.

5.3 Life issues

The previous work at Sandia and KPI revealed a number of life issues with the 8-micron-fiber wicks tested at Sandia. These include the following areas of concern [31]:

- Wick Compression: The liquid in the wick is in tension, and applies a net compressive loading perpendicular to the wick surface. This loading, coupled with high temperatures and limited creep strength of the wick fibers, resulted in significant crushing of the wick, which led to reduced wick performance. KPI addressed this with substantial characterization, which led to the selection of a 30-micron fiber diameter.
- Wall-wick bond: While the wick sinters well to itself, the wall-wick bond on some samples was limited. The wall is typically a different material than the wick. The wall-wick bond characteristics were improved in the change to the thicker fiber, as well as careful modification of the sintering processes.
- Local wick rupture: Some occasions of local wick rupture were encountered. This appeared to be a combination of wick crushing and wick flow characteristics, leading to local pockets of trapped vapor, which could then tear the surface layers of the wick. This is in part addressed with the more robust wick structure. In addition, periodic —vents" are formed in the wick, providing a robust path for escape of vapor.
- Oxygen contamination: The heat pipe has a single point of lowest pressure, to which non-volatile contaminants are swept. Oxides are particularly harmful, as they reach concentrations at which the

stainless steel fibers, at temperature, are corroded rapidly, resulting in loss of wick structure. Sandia developed wick processing and cleaning methods [25] that have eliminated oxygen as a concern, and which have been adopted by others in the heat pipe community [27].

- Other contaminants: Other, non-corrosive contaminants are swept to the low pressure point, and can lead to plugging of the wick. While this has been observed, typically as a pellet of copper at the low pressure point, the pellet has been small enough to not impact performance. The copper comes from residual brass on the fibers from the fiber drawing process. The larger fibers will have smaller surface area, limiting the amount of contamination. Reflux processing of the pipe also reduces the levels of all soluble non-volatile contaminants.

These key life-reduction issues have been addressed in detail by Dr. Baturkin in the KPI IPP project [32], but with some impact on system performance. However, no long-term durability testing of the wicks in a strong reflux environment has been performed. In addition, according to our current wick models, we anticipate that we can restore some of the wick capacity while maintaining the durability features. The performance restoration can be through graded wick approaches as well as mid-sized fiber diameters not considered in prior studies.

5.4 Approach

We will perform long-term (20,000 hours) steady state testing of the proposed wick candidate, with thermal, liquid, and vapor flux rates similar to the full scale receiver. These tests will be monitored non-destructively for wick physical changes (gross thickness in the heated zone) through x-ray testing. Prior to selection of a final wick, mercury intrusion (porosimetry) will be performed on several candidate structures, all variations of the prior Baturkin work. Based on this data, a wick performance model can be run to indicate the performance margins at the full-scale receiver operating conditions. The wick with the highest operational margins will be incorporated into the test device. Our test device allows incorporation of two different wicks, which can be independently tested for short-term performance. The successful short-term wick will be tested unattended in the durability test rig.

5.5 Life Test

Sandia developed a heat pipe wick durability test rig that simulates conditions of a full-scale receiver [30]. Prior capsule tests that were high temperature but limited reflux and limited wick area failed to duplicate the durability and performance problems observed on sun. The bench scale test, Figure 21, operates unattended. The flux level is up to 60W/cm², supplied by quartz lamp arrays. The height above the pool provides local wick pressures similar to those seen in the full-scale receiver. Both the back wall (condenser) and front wall (transport and evaporation) are covered with wick, providing sufficient surface area to test for contamination introduced by the wick structure. The system is passively cooled, and can be augmented with a fan to maintain near-full-power as ambient temperatures change.

Prior development and testing indicates that this durability test accurately demonstrates typical failure modes seen in full scale tests of the same wick assemblies, including corrosion, plugging, and wick compression.

The test capability was dismantled in the early 2000‘s when the DOE program was terminated. The DAQ equipment, while still available, is old and unreliable, and unsupported by modern computers. The test capability will be restored using modern DAQ tools, based on the successful test capability previously utilized. The lamp arrays, cooling systems, lamp controls, and test bunkers are still available, so hardware purchases are limited to DAQ systems.

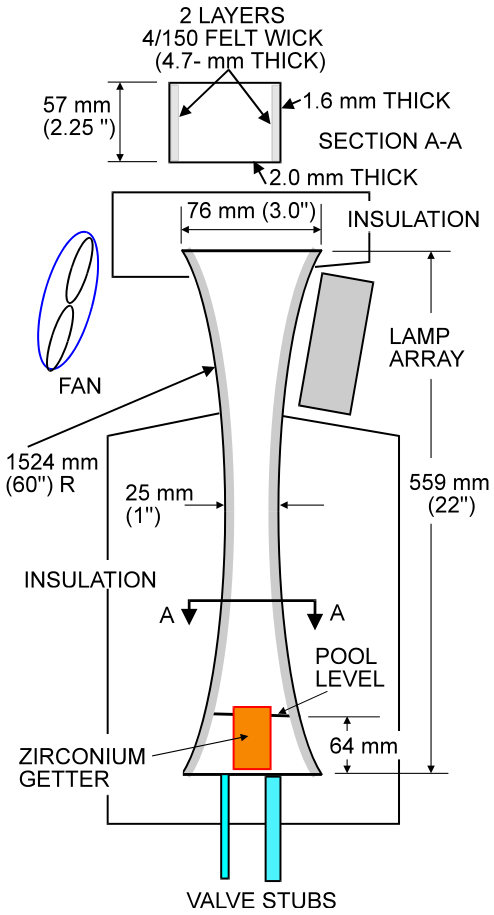

Figure 21. Sandia durability bench scale heat pipe system

5.6 Risk Assessment

Due to timescale and funding limitations, the heat pipe development program is actually a durability demonstration of previously-developed technology with minor modifications. The schedule does not allow for further wick development trials and testing. A failure of the proposed wick assembly, depending on the failure mode, could be a serious setback for dish storage development.

During the wick fabrication, about a half dozen samples will be manufactured and tested with mercury porosimetry. This will ensure that the fabrication techniques are correctly re-established, and will allow a small amount of modification to the permeability and porosity of the samples through various sintering parameters.

Should the wick fail durability testing, a fallback position for short-term operation could be the Thermacore/ACT approach with sintered nickel powder wicks. This approach has limited throughput capability, relies on non-self-priming arteries, and has some durability issues (cracking, bonding) as well. However, utilization of such wicks would allow demonstration of other aspects of the storage system in short-term, lower power situations. A high performance wick development effort would be required prior to production.

This page intentionally left blank

6 PCM STORAGE

6.1 Storage Media Properties

A critical element of the dish storage system is the Phase Change Material (PCM), which must be selected, characterized, and tested for compatibility. The PCM needs differ strongly from efforts already underway for tower and trough systems, due to the higher temperature (750-800°C) and the limited space and mass on the tracking portion of a dish system. The phase-change storage media must be selected first, as this choice affects most of the system-level optimizations. The most critical parameter is the melting point temperature, as this sets the operating temperature for the entire system, and has a direct impact on the engine performance (lower temperature) or on life issues (higher temperature). Table 3 indicates the high-level selection criterion for the PCM. In addition to melting point, the volumetric and gravimetric densities are critical because the system is mounted on the dish structure. Finally, thermal conductivity, particularly in the solid phase, will strongly influence the optimized layout of heat pipe heat exchangers in the PCM bed.

Table 3. Selection Criterion for PCM

Criterion	Implications
Melting Point	Needs to match Stirling cycle. Ideally between 750 °C and 800 °C.
Heat of Fusion	Equal to the gravimetric density, determines the mass of the storage media needed to meet the storage requirements. Implications of system support structure and system balance.
Volumetric Storage Density	Gravimetric storage density times the mass density of the material. This impacts the size of the storage media, and therefore the quantity of containment material as well as the thermal losses by conduction.
Thermal Conductivity	Low conductivity leads to higher temperature drops on charge and discharge, impacting exergetic efficiency. Can be mitigated with a higher density of heat pipe condensers and evaporators, but at a system monetary cost.
Material Compatibility	The PCM must have compatibility at temperature with reasonable containment materials over long periods.
Stability	The PCM must not break down over time at temperature. This includes major changes such as separation of components and changes in composition, as well as minor issues such as outgassing and changes in melting point.
Coefficient of Thermal Expansion	This can impact the design of the containment and may require volumetric accommodation of size changes with temperature.
Phase Change Volumetric Expansion	This can lead to voids, increasing thermal resistance through the solid phase, and can potentially cause damage to the heat pipe tubes.
Vapor pressure	Related to stability, a high vapor pressure can lead to containment issues and/or higher cost for containment.
Cost	The cost of the PCM directly impacts the LCOE of the system.

We considered a large number of potential PCM candidates (complete compilation included in Appendix A). From this, we have identified some candidates of interest, listed in Table 4. The quality of the data available in the open literature varies. Generally, though, we were unable to find reliable data on the

thermal conductivities of the liquid and solid phases of the metallics. We made order-of-magnitude guesses as to the conductivity, based on the solid-phase conductivity of the constituents. This is done to indicate the substantial advantage of metallic over the salts, but these numbers should not be used in any analytical context. Even melting point data varied somewhat. However, this table does indicate that several potential PCM's exist, and that further lab work is needed to demonstrate that the properties are acceptable. We found that little is published at these temperatures concerning compatibility with containment vessels of interest.

Table 4. Potentially promising PCM candidates and their properties of interest

PCM	Melting Point (°C)	Mass(kg for 6 hr)	Vol (m^3 for 6 hr)	Conductivity (solid, W/mK)
NaCl	801	2980	1.1	1.59
H755	755	3090	1.0	0.589
Cu-0.30Si	803	7309	1.3	300[a]
Si-0.35Cu-0.28Mg	750-770	3402	1.75	200[a]
Mg - 0.38Si - 0.06Zn	800	4585	-	100[a]

[a]Conductivity is estimated order of magnitude based on constituents

Based on this preliminary screening, several metallics show promise for PCM for dish storage. It must be stressed that insufficient data is available on these metallics, particularly as it relates to materials compatibility with potential containment materials. However, the known and estimated thermophysical properties give promise that a solution can be found. The need for compatibility testing cannot be over-stressed.

7 SYSTEM LAYOUT (STORAGE INTERFACE CONSIDERATIONS)

7.1 Background:

As described earlier, the PCM storage will be placed between the solar heat-pipe receiver, located near the focal point of the concentrator, and the engine, located on the back of the dish structure. The PCM storage vessel is proposed to be mounted on the back of the main dish structure, co-located with the engine package. This layout has the advantage of balancing the concentrator, and keeps only the relatively light receiver on the cantilevered support boom.

The PCM storage vessel serves two functions – it is a heat exchanger between the solar receiver heat-pipe and the engine heater head heat-pipe, and of course contains the PCM storage material. The vessel assembly would consist of the receiver-to-PCM heat-pipe and its associated header on one end, and the engine-to-PCM heat-pipe, with its associated header on the other end. It would look like a tube-and-shell heat exchanger, but the "tube" section would be two separate assemblies that are interlaced with each other. A section of this heat exchanger is illustrated in Figure 22. The red pipe signifies one heat-pipe assembly, while the blue pipes signify the second heat-pipe assembly. The "shell" side of the tube-and-shell heat exchanger contains the PCM material.

In this section, we consider a high level model of the heat pipe/PCM interfaces. The purpose of this is to determine whether a "feasible" number and configuration of tubes within the PCM can provide suitable heat transfer and limit the exergy losses to about 5%. We consider a representative salt and a representative metallic for this parametric study. It is important to note that when considering low-conductivity PCM materials, a purely conductive model such as this will likely significantly under-estimate the thermal transport, and free convection of multiphase systems must be considered in a more detailed modeling effort [33]. In this simplistic approach, we are merely concerned about the temperature drop apparent across the PCM module, for comparison to our exergy analysis.

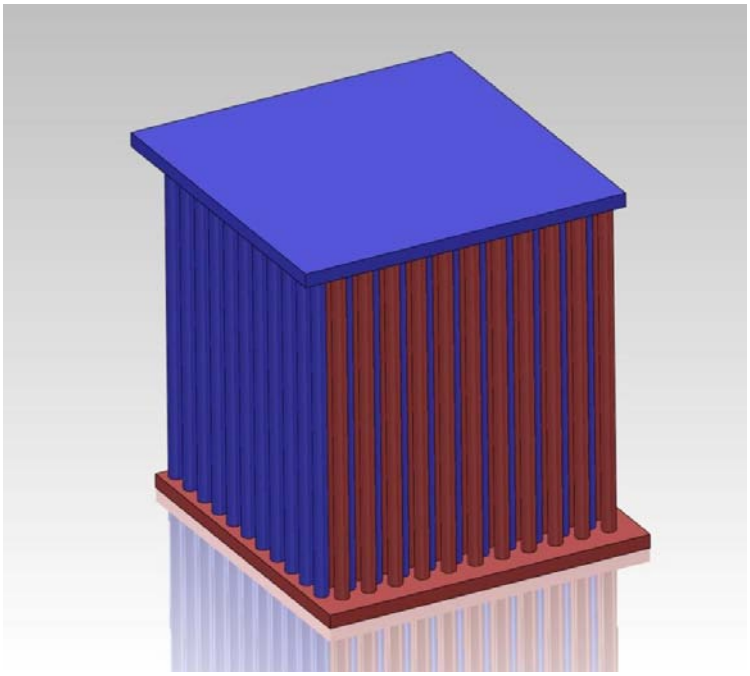

Figure 22. Schematic representation of PCM storage vessel with heat pipe grid

7.2 PCM Materials:

The choice of the PCM material is critical to optimal system operation. Stirling engines run progressively more efficiently as the heater head temperature increases. However material life typically limits this hot-end temperature to about 800 ºC.

We selected NaCl and Cu-0.30Si as candidate PCM materials for this study. These two selections contrast a readily available and cheap salt with a more exotic metallic with greatly increased thermal conductivity.

Unfortunately, quantifying the thermal conductivity of copper-silicon proved to be difficult in the available literature. Documents were found that measured thermal storage capacities, but surprisingly did not measure conductivity. At this point, only conductivities for up to 4% silicon and up to 200ºC were found. This particular eutectic of interest is 16% silicon. In the analysis we chose a constant bounding value of 50 W/m-K, which may be significantly lower than some of the potential metallics. The important point was that it is more than an order of magnitude greater than the conductivity of NaCl.

7.3 Approach and Finite Element Model (FEM):

Finite element modeling of the entire heat exchanger would be tedious and unnecessary, as there is a repeating pattern of heat pipes and PCM material. We chose to model a representative section of the PCM/Heat Pipe array. This approach does ignore edge effects that would occur near the perimeter of the vessel. A unit cell can be representative of this repeating pattern. A unit cell consists of four quarter sections of tubes in the receiver-to-PCM heat-pipe and one central heat-pipe of the PCM-to-engine heat-pipe (or vice-versa). The unit cell is shown in Figure 23.

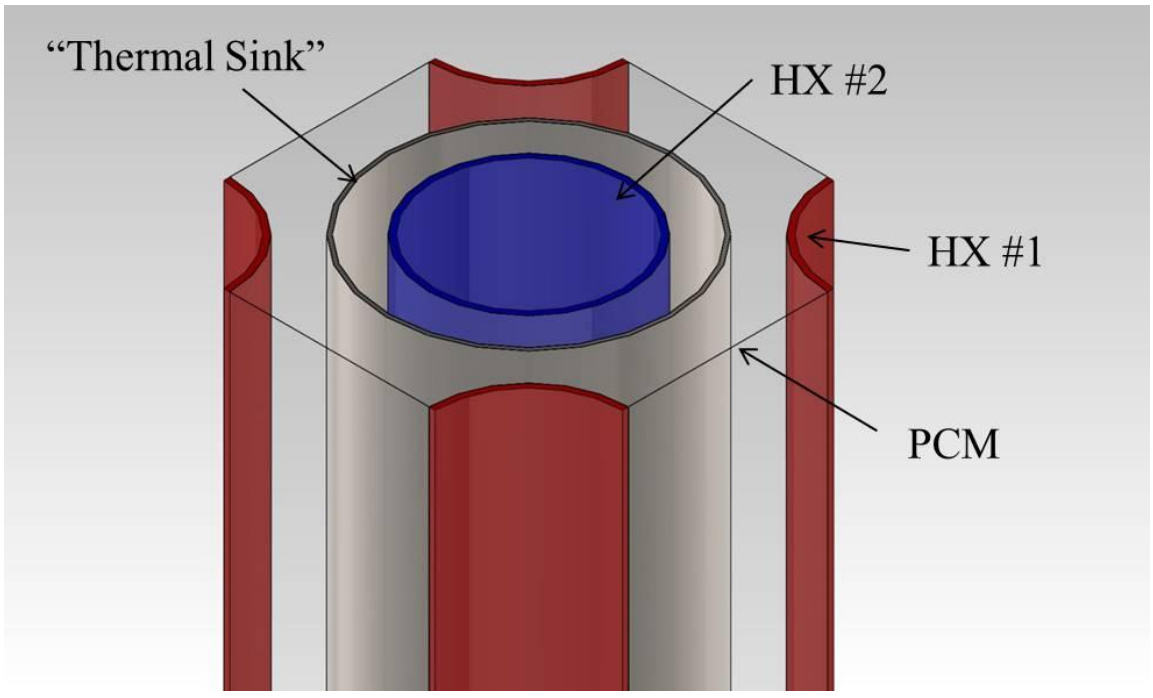

Figure 23. Unit Cell of a PCM Storage Vessel

A finite element model of a unit cell was generated using SolidWorks™ 3-D CAD software. SolidWorks Simulation ™ was used to analyze the assemblies. The item labeled ―thermal sink" in Figure 23 is an idealized position located centrally between the two sets of heat pipes that act as a thermal storage sink when the solar multiple is more than one. In the FEM, heat is extracted in this zone to simulate energy being stored in the PCM as latent heat.

Because the heat-pipes operate isothermally, there is very little temperature difference along the length of the pipe. This is not entirely true because convection would be present and would affect heat transfer along the pipe length. However, as a first order analysis, convection and edge effects were neglected. With these assumptions, the problem is reduced to a 2-D analysis. A short section of the unit cell used in the analysis is shown in Figure 3. It is important to note that we considered ONLY conduction through the PCM material, and no free convection was considered. This is a bounding case. While it may be accurate for the solid phase, some studies have shown that ignoring convection can reduce heat transfer by as much as a factor of 18, though for grossly different configurations. Therefore, this simplified model should only be considered preliminary scoping. It is likely that higher conductivity PCM's (metallics) will realize less benefit from natural convection heat transfer enhancement.

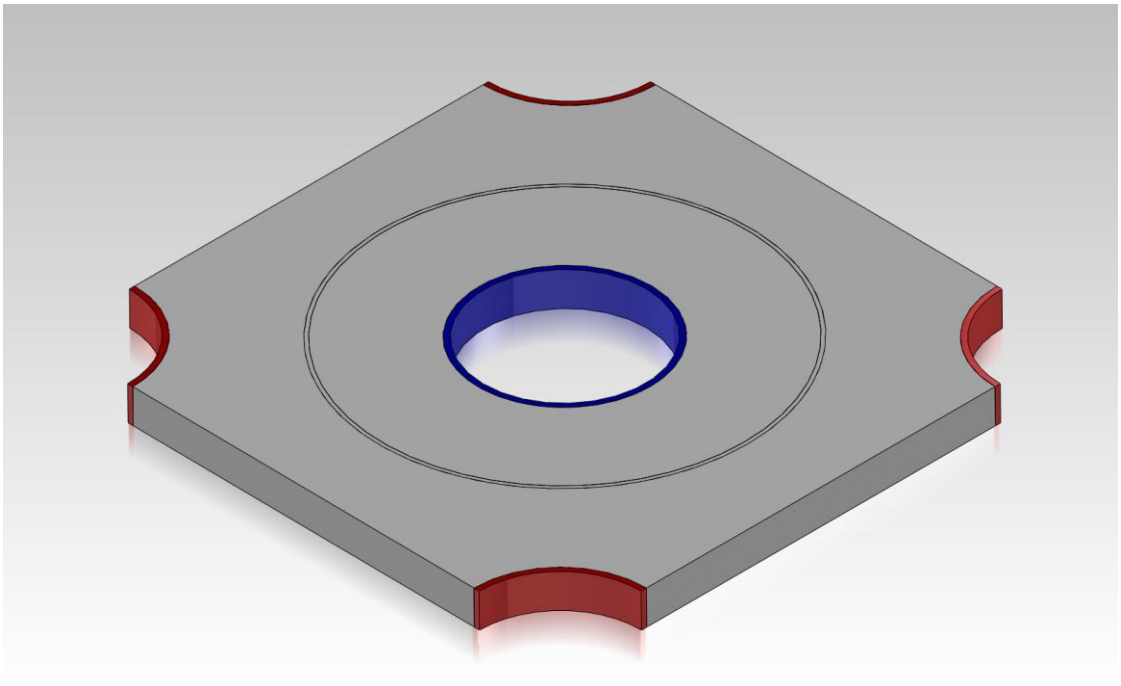

Figure 24. Unit Cell of a PCM Storage Vessel, 2-D Slice.

Some FEA model details and input conditions include:

- 65 kW absorbed into the engine-side heat-pipe – this value is ratioed for the number of unit cells
- Thermal storage – 390kW-hr – from 65 kW * 6 hours of storage
- Tubes modeled as 0.060" wall Haynes 230 tubes
- Power is extracted midway through PCM material for solar multiples > 1 (see description above)
- Power extracted on inner heat-pipe tube

- 800ºC boundary condition placed on 4x quarter heat-pipe sections

A parametric study was performed using this simplified model. The following parameters were varied:

- PCM- NaCl or copper-silicon eutectic estimate
- Heat-pipe diameters: 0.5", 1", 1.5", 2.0"
- Tube spacing:
  - NaCl: 1.50*D, 1.75*D, 2.0*D, 2.25*D
  - Copper-silicon: 2.0*D, 3.0*D, 4.0*D, 5.0*D
- Solar Multiple: 1.0, 1.25, 1.5, 2.0

As heat is conducted across one heat-pipe to the other, there is an associated temperature drop. A simple exergy analysis (earlier section) indicted that the maximum desired temperature drop is 45ºC. The smaller the temperature drop, the greater the performance margin. This value of 45ºC was used to declare if a particular layout would be deemed acceptable.

7.4 Results:

The results for the NaCl PCM are shown in Figure 25. This graph shows the temperature drop from the receiver-to-PCM heat-pipe to the PCM-to-engine heat-pipe. The dark horizontal line is the 45ºC acceptable cutoff described above. The labels correspond to the number of heat pipe tubes needed for each heat-pipe assembly that has a length of 1-m. As the graph indicates, very small temperature drops can be attained with tight tube spacing, but contain a large (absurd?) amount of tubes. Conversely, fewer tubes lead to greater temperature drops. To meet the 45ºC cutoff across the entire range of solar multiples (up to 2), almost 400 unit cells, or pipes are needed for each heat-pipe assembly.

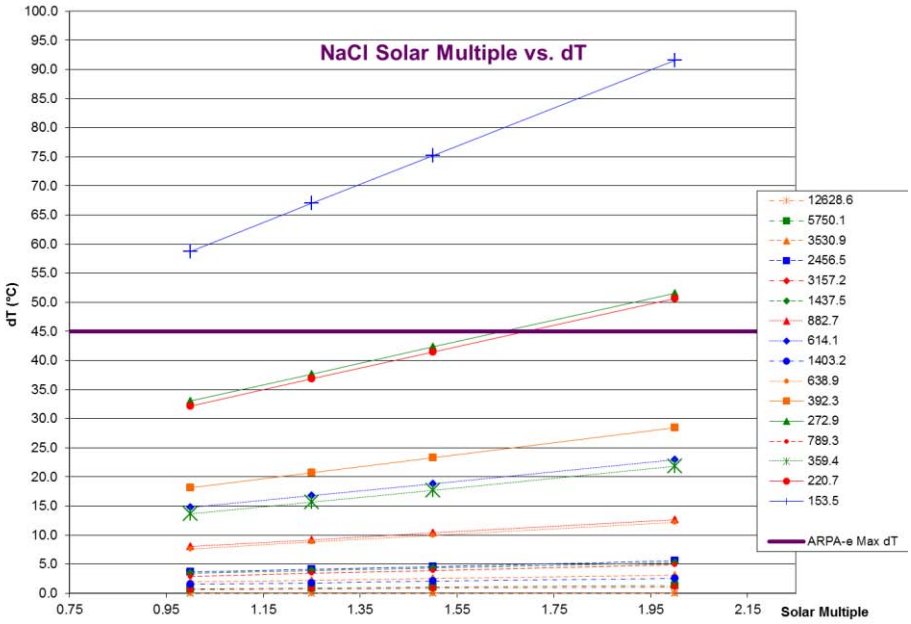

Figure 25. Temperature Drop Versus Solar Multiple for NaCl.

Figure 26 shows a similar graph for a copper-silicon PCM. Due to the difference in thermal conductivities, the metal PCM allowed a greater tube spacing than did the NaCl PCM. The implication is

that a PCM with higher conductivity allow far fewer pipes. Figure 26 indicates that only 32 pipes are needed in each heat-pipe assembly – a far fewer number than for NaCl. Fewer piece-parts results in lower material and fabrication costs, which can be traded off against the cost of the PCM.

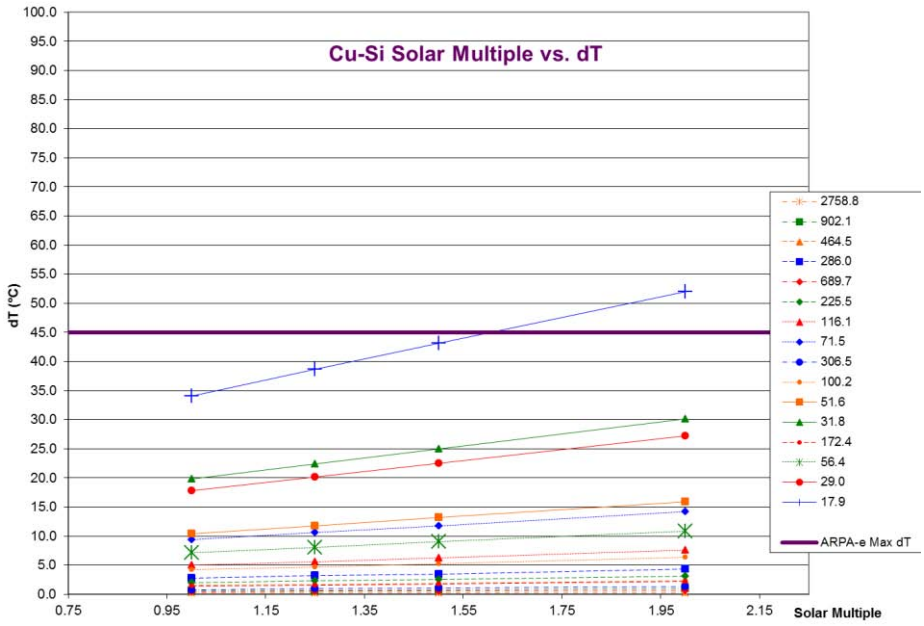

Figure 26. Temperature Drop Versus Solar Multiple for Copper-Silicon.

7.5 Conclusions:

From the results above, some conclusions are:

- A metal eutectic PCM greatly outperforms a salt PCM due to superior thermal conductivity. This is approximately an order of magnitude difference in number of heat pipe tubes.
- These results imply that copper-silicon PCM has the benefit of greatly reduced PCM vessel costs.
- Further material data and availability investigation is needed to confirm copper-silicon is a viable PCM.
- A potentially feasible physical configuration is shown with the metallic PCM system.
- A more detailed model that includes natural convection enhancements to the heat transfer should improve the lot of the NaCl option.

This page intentionally left blank

8 IMPACT ON DISH DESIGN

8.1 Background:

The typical solar dish system consists of a parabolic mirrored surface attached to a beam structure. A receiver/engine package is mounted near the focal point of the concentrator, supported by a bipod, tripod, or boom structure. The dish structure is tied to a tracking system which moves the mirror and engine package in two axes, azimuth and elevation. This tracking system may consist of an elevation axis nested on top of a circular track for azimuth, or contain both axes on top of a fixed pedestal. For cost reasons, a pedestal is usually chosen. Some layouts place a full parabolic structure in front of the azimuth axis – the Test Bed Concentrators at Sandia's NSTTF is an example (Figure 27). The disadvantage of this layout is that the center of gravity is forward of the mirror surface, therefore the structure is cantilevered from the elevation axis. This is not a balanced system, and places high loads on the elevation axis drive components.

Figure 27. Test Bed Concentrators at Sandia, showing a fully cantilevered drive system.

To balance the system structurally, a common layout is to use a pedestal mount that extends upward just forward of the mirror surface, providing an elevation pivot at or near the center of gravity of the dish rotating system. However, so the mirrors do not interfere with the pedestal at high sun elevations, the lower section of the mirror needs to be removed. From a structural viewpoint, this notch (commonly referred to as the "keyhole" or "pedestal slot") opens the previously closed structure, making it significantly less stiff, resulting in mirror facet pointing errors as the gravity vector with respect to the structure changes throughout the day. Since small deviations from a true parabolic shape make large differences in the receiver flux distribution, the structure must be stiffened to compensate for the open structure. An example of a keyhole dish structure is shown in Figure 28, the Sandia Advanced Dish Development Systems (ADDS).

Figure 28. Balanced dish design with keyhole to accommodate pedestal.

The cost and simplicity of the pedestal layout can be combined with the stiffness of a closed structure if the center of gravity can be moved behind the pedestal. We propose to use the mass of the PCM system as a counterweight – it can be mounted on the hub of the structure, placing the center of gravity between the PCM system and the parabolic dish structure.

To get an idea of the stiffness differences between an open and a closed structure, both structures were modeled with a simplified representative structure.

8.2 Approach and Finite Element Model (FEM):

Finite element models of both an open and a closed parabolic dish structure were generated using SolidWorks™ 3-D CAD software. SolidWorks Simulation ™ was used to analyze the assemblies.

Instead of modeling the entire system from the ground up, only the structures downstream of the mounting hubs were modeled. Each model consisted of a hub structure, the supporting beam structure, the receiver boom, and the receiver. Although there are some shortcomings of not including the pedestal

and pedestal-to-hub transition details, the models would be useful in estimating the stiffness differences between the open and closed structures. Some model details include:

- Hub, radials, circumferential beams, and receiver boom were modeled with common structural shapes, and meshed with beam elements
- Mirror surface modeled as a continuous surface, and meshed with shell elements
- Mirror was bonded to radials at discrete locations (roughly corresponding to mounting pads)
- Receiver was modeled as a 200 lb block located at the end of the receiver boom
- Model was fixed at rear of hub – this is normally a very stiff area as it ties into the transition area from the pedestal
- Loading: 1-g gravity load

The approach was to generate a closed structure that would be stiff enough to produce acceptable deflections in the mirror surface. A goal was to allow mirror surface rotations up to approximately 1 mrad. A similar model was then made for the keyhole design. The notch implied the hub structure would be open, and the lower radial beam (and corresponding mirror surface) could not be included. The missing mirror area was compensated with using a slightly large diameter mirror surface.

8.3 Results:

Figure 29 shows the model of the full structure. Square tubing was used in the hub area and round tubing was used in the radials and receiver boom.

Maximum mirror rotations for this case were about 1 mrad (Figure 30). However, most of the mirror area was within 0.2 mrad. Figure 30 shows the mirror rotations about one of the two axes on interest.

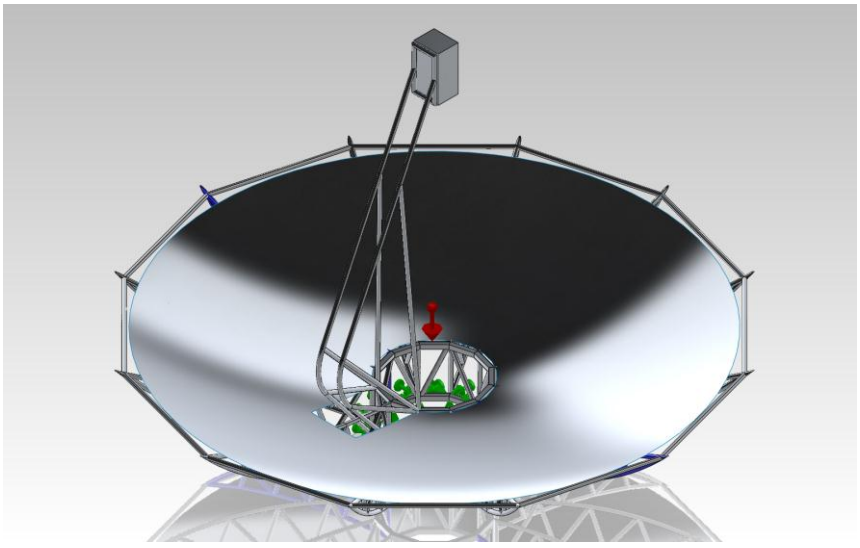

Figure 29. Fully closed structural model

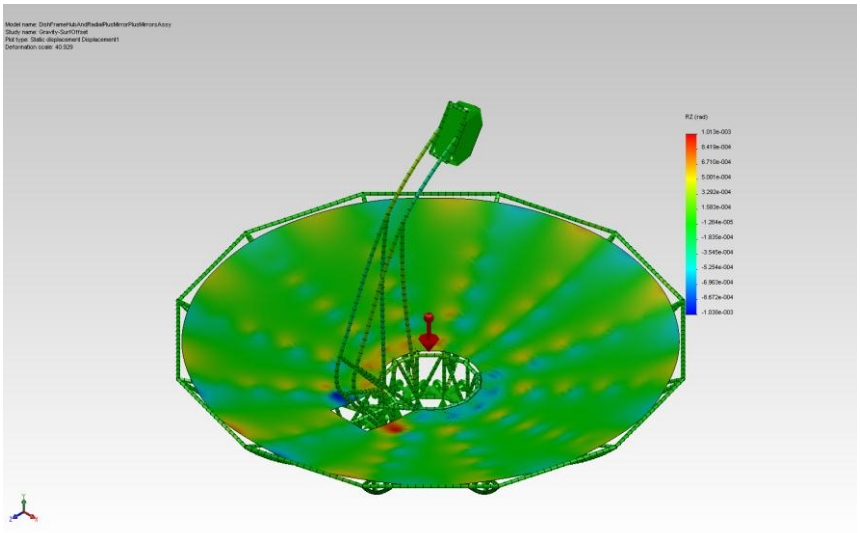

Figure 30. Mirror surface rotations for fully closed structure model.

Figure 31 shows the model of the keyhole structure dish system. As mentioned earlier, the mirror diameter was increased to compensate for the mirror area lost due to the keyhole.

Maximum mirror rotations for this case were about 10 mrad. However, most of these large deformations were in the keyhole area. As with the most of the mirror area in the closed structure, much of the mirror area distortions were much better -- within about 2 mrad. Figure 32 shows the mirror rotations for this case.

Comparing the mirror errors between the two models, the keyhole model is approximately an order of magnitude worse than the fully closed structure (2 mrad versus 0.2 mrad for a large percentage of the surface area).

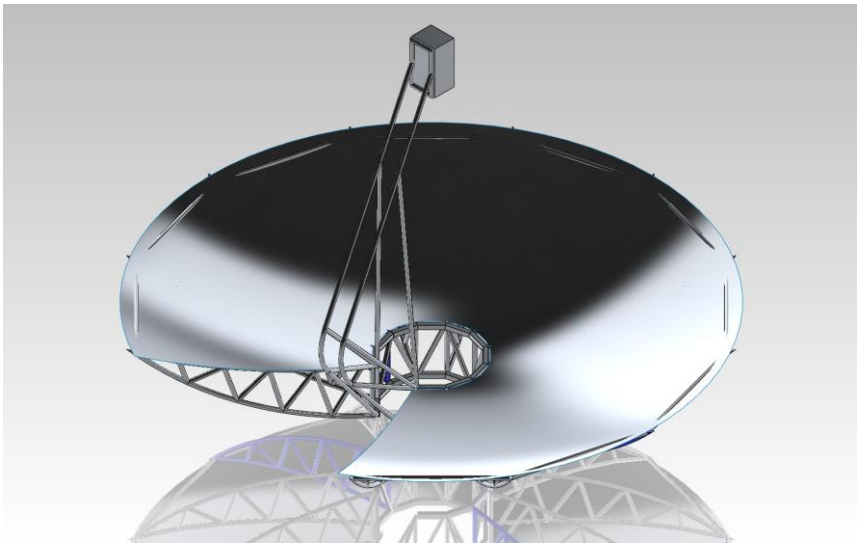

Figure 31. Keyhole structure model.

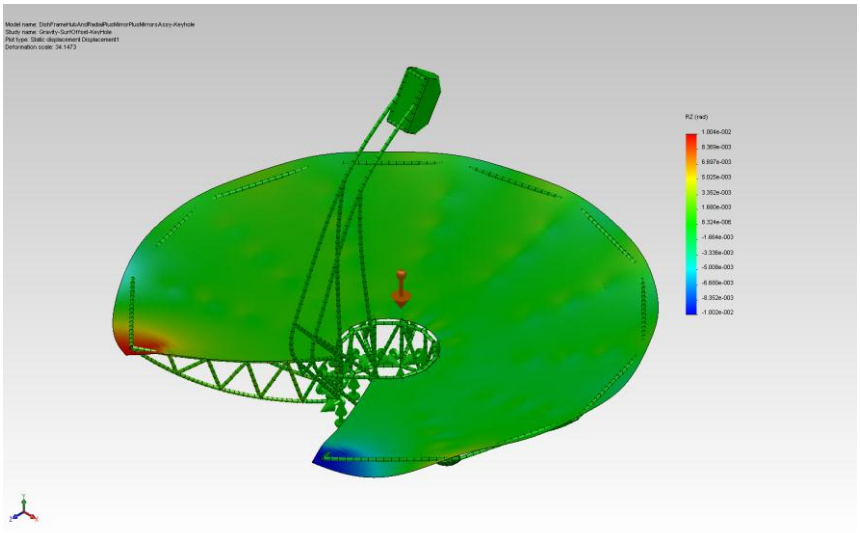

Figure 32. Mirror surface rotations for keyhole structure model.

These models were constructed with the approximate area for driving a 25 kWe system. For higher solar multiples, the effect would be even more dramatic, as the diameter of the dish would increase proportional to the root of the solar multiple. For a solar multiple of two, the dish would be approximately 15-m, significantly larger than the 11-m structures modeled.

A significant cost savings would be realized by eliminating the typical keyhole slot in the dish structure. Smaller members could be used to get the same net system stiffness, reducing the weight and therefore cost of the system. In addition, the lower structural weight would reduce the loads on the elements, further reducing the deflections due to gravity loading. A rough estimate to achieve an order of magnitude change in stiffness is a factor of two in mass, and therefore in structural material costs.

8.4 Conclusions:

From the results above, some conclusions are:

- A PCM storage system mounted on the rear of the dish can balance the system on a cost-efficient pedestal design. This allows elimination of the keyhole, which significantly increases the dish stiffness.
- Given a required dish stiffness, closing the keyhole can reduce the structure cost significantly.
- The addition of a rear-mounted engine and storage unit may result in significant system cost savings that can offset some of the storage system costs.

This page intentionally left blank

9 DEVELOPMENT NEEDS

Having reviewed the proposed concept in the development of these models and studies, there are a number of areas that require development before these systems could be deployed on production dish Stirling systems. We have broken these development needs into key technology areas and developmental areas. The key technology areas include areas that need fundamental development, and which, if unsolved, would present a significant technical barrier (show stopper). The development areas are areas that need to be solved, but are seen as design, integration, or deployment issues rather than fundamental barriers.

The key technology areas should be addressed by the DOE development program, in order to eliminate technical barriers to incorporation of storage on dish Stirling systems. During the research in these areas, the staff should be cognizant of the developmental areas, and aware if any of these should be escalated to a key technical area.

The key technical areas identified include:

- Solar heat pipe wick development and durability testing. A high performance wick capable of up to 100kWth throughput and peak fluxes approaching 100W/cm² must be demonstrated. If current advanced wicks prove insufficient, further development may be needed. We believe a variation of Sandia felt wick technologies, developed in past DOE work, should prove sufficient.
- PCM selection. Significant gaps exist in the data for potential PCM‘s, including thermal conductivities, melting points, and volume change during melting, among other parameters. A suitable PCM (or several) needs to be selected and characterized.
- PCM compatibility. At elevated temperatures, compatibility issues are amplified. The PCM compatibility with potential cost-effective shell materials must be considered and tested. The shell materials also need to be compatible with liquid sodium and air.
- PCM system thermal performance. The PCM/heat pipe combination is a complex thermal system, which is not well characterized with simple conductivity models. We need to fully understand the heat transfer modes and mechanisms within the PCM during cyclic charge and discharge, in order to optimize the system performance and cost. In addition, we must understand PCM/shell physical interactions, particularly due to freeze/thaw volumetric changes.
- System demonstration. The proposed novel configuration, once designed, will require a proof of concept demonstration to verify analytical findings, and to increase value of the system design, leading to commercial application. Within the context of expected budget and time, an electrically-fired bench scale system with heat pipe input and output, and PCM storage, is a feasible demonstration, and can investigate performance, losses, and compatibilities, and can be used to confirm design and development tools and models.
- System modeling. Further refinement of the systems model can be used to justify storage in a dish Stirling context. In particular, the interaction of storage systems and TOD value profiles should be further investigated to provide guidance for the utilities to place value on the storage concept. Refinement of the loss and operational mechanisms will help make a credible model for detailed engineering tradeoffs and design.

The following developmental areas should be considered during the research phase, but are likely best left to the product integrator. These areas may be specific to the product to which storage is applied, or may simply be beyond the scope of the proposed work and schedule. These areas should be appropriately addressed by the manufacturer, or if identified as an increased risk, in follow-up work supported by the DOE.

- Engine/Heat Pipe interface. This is not a simple interface, and must account for differential expansion of various components. However, it is highly specific to the engine design, and thus best performed by the manufacturer.
- Liquid Metal Pump. The LM pump is likely to be an electro-magnetic (EM) pump. Commercial designs exist, but tend to be high flow systems. Sandia has built some low flow simple pumps. It is likely that a commercial company could adapt existing technologies to the needs of this system. The EM pump returns the sodium to the receiver cavity area.
- Thermal expansion issues. A significant length of pipe or tube is proposed to join the receiver to the PCM containment on the rear of the dish. Intelligent engineering can be used to minimize the stresses induced through the very large temperature range of the pipe. This should be done, if possible, without bellows or rotating joints, in order to minimize thin walled containment. It is likely that long pipe runs can be arranged to absorb the expansion through elastic deformation.
- Freezing and startup. The system must be designed to successfully recover from freezes during non-operation. Liquid management during shutdown is critical, and may not be passive. Recovery from abnormal shutdown must be considered.
- Ratcheting. Any thermo-mechanical ratcheting must be considered in the final design.
- Management of full storage. While shedding is likely needed on some days, it is not clear how simple this is. It may consist of simply coming off-sun periodically, in a pulse-width-modulation scheme of thermal input. Other shedding mechanisms may be considered.
- Safety. Considerable quantities of hot, nasty elements are contemplated. It is unlikely that the sodium quantity will exceed the EPA-reportable 10 pounds per device. However, due to the reactivity of the sodium, and potentially of the PCM, chemical safety must be considered. In addition, thermal safety issues must be considered.
- Dish Redesign. The dish system will have to undergo extensive redesign to support the storage unit and engine on the rear structure, and also to take advantage of the benefit of closing the pedestal gap. This work is best left to the dish developer.

10 LITERATURE CITATIONS

[1] Andraka, C. E. and Powell, M. P., 2008, "Dish Stirling Development For Utility-Scale Commercialization," 14th Biennial CSP SolarPACES Symposium, Las Vegas, NV.

[2] Cleanergy, Inc, "Utility Scale Solar Parks", http://www.cleanergy.com/solar-engines/utility-scale-solar-parks/

[3] Igo, John, and Charles E. Andraka, "Solar Dish Field System Model For Spacing Optimization", ES2007-36154, Proceedings of ES2007,ASME, Energy Sustainability 2007, June 27-30, 2007, Long Beach, California.

[4] Sargent & Lundy Consulting Group, 2003, "Assessment of Parabolic Trough and Power Tower Solar Technology Cost and Performance Forecasts," SL-5641, Chicago IL.

[5] Public Utilities Commission of the State of California, Resolution E-4442, December 1, 2011

[6] Andraka, C.E., Stechel, E., Becker, P.H., Messick, B., "White Paper on Dish Stirling Technology", prepared for DOE EERE, April 20, 2011

[7] Andraka, C.E., "High Performance Thermal Storage Solutions for Dish Stirling Systems", ARPA-E proposal in response to HEATS FOA call, Control Number 0471-1578, July 18, 2011

[8] Andraka C.E., Rawlinson K.S., Moss T.A., Adkins D.R., Moreno J.B., Cordeiro P.G., Johansson S., Gallup D.R., "Solar Heat Pipe Testing of the Stirling Thermal Motors 4-120 Stirling Engine" , SAND96-1424C, IECEC 1996 Washington DC, Aug 1,1996

[9] Adkins D.R., Moss T.A., Andraka C.E., Andreas N.H., Cole H.M., "An Examination of Metal Felt Wicks for Heat-Pipe Applications" , SAND94-0657C, Solar Engineering 1995, Proceedings of the ASME Solar Energy Division, Maui Hawaii, April 1995, Mar 19,1995

[10] Andraka C.E., "Solar Heat-Pipe Receiver Wick Modeling" , 98-2836C, ASME SED conference, Maui HI, April 11-16, 1999, Apr 11,1999

[11] Baturkin, V; Zaripov, V., Andraka, C.E., Moss, T.A., "Features Of Fabrication Technology And Properties Of Wicks Of Heat Pipe Receivers For Solar Dish/Stirling Systems", Proceedings of ISEC2005: 2005 Solar World Conference, August 2005.

[12] "Concentrating Solar Power Industry Projects", DOE Solar Energy technologies Program website, http://www1.eere.energy.gov/solar/csp_industry_projects.html.

[13] Thermal Power Systems Advanced Solar Thermal Technology Project, Advanced Subsystems Development Second Semi-Annual Progress Report, DOE/JPL-1060-6, Jet Propulsion Laboratory, California Institute of Technology, Pasadena CA, pp3-1 to 3-40, Nov 15, 1978.

[14] Fujita, T., Birur, G.C., Schredder, J.M., Bowyer, J.M., and Awaya, H.I., "Comparison of advanced thermal and electrical storage for parabolic dish solar thermal power systems," 17th Intersociety Energy Conversion Engineering Conference (IECEC), Los Angeles, CA August 8-13, 1982.

[15] Stearns, J., "Solar Stirling receiver alternatives for the terrestrial solar application," DOE/JPL-1060-96, April 30, 1986.

[16] Andraka, C.E., "Cost/Performance Tradeoffs For Reflectors Used In Solar Concentrating Dish Systems," ES2008-54048, Proceedings of ES2008, ASME, Energy Sustainability 2008, August 10-14, 2008, Jacksonville, FL.

[17] Kolb, G.J., Finch, N., Ho, C., "Novel Heliostat Design", SNL CSP AOP kickoff meeting, November 10, 2011, Albuquerque.

[18] Shaubach, R. M. and Gernet, N. J., "Sodium Heat Pipe with Sintered Wick and Artery: Effects of Noncondensible Gas On Performance", AIP Conf. Proc. 246, 1153 (1992)

[19] G.S. Hwang, E. Fleming, B. Carne, S. Sharratt, Y. Nam, P. Dussinger, Y.S. Ju, M. Kaviany, "Multi-artery heat-pipe spreader: Lateral liquid supply", International Journal of Heat and Mass Transfer, Volume 54, Issues 11-12, May 2011, Pages 2334-2340, ISSN 0017-9310

[20] Testing results at Sandia National Laboratories

[21] Lin, Fang-Chou; Liu, Bing-Han;, Huang, Chi-Ting; Chen, Yau-Ming, "Evaporative Heat Transfer Model of a Loop Heat Pipe with Bidisperse Wick Structure", International Journal of Heat and Mass Transfer, Volume 54, Issues 21-22, October 2011, Pages 4621-4629, ISSN 0017-9310, 10.1016/j.ijheatmasstransfer.2011.06.015.

[22] B. Suman, "Microgrooved Heat Pipe", In: Thomas F. Irvine and James P. Hartnett, Editor(s), Advances in Heat Transfer, Elsevier, 2009, Volume 41, Pages 1-80, ISSN 0065-2717

[23] Zuo, Z.J.; North, M.T.; Wert, K.L.; , "High heat flux heat pipe mechanism for cooling of electronics," Components and Packaging Technologies, IEEE Transactions on , vol.24, no.2, pp.220-225, Jun 2001
doi: 10.1109/6144.926386

[24] Vasiliev, L., Lossouarn, D., Romestant, C., Alexandre, A., Bertin, Y., Piatsiushyk, Y., Romanenkov, V., "Loop Heat Pipe for Cooling of High-Power Electronic Components", International Journal of Heat and Mass Transfer, Volume 52, Issues 1-2, 15 January 2009, Pages 301-308, ISSN 0017-9310, 10.1016/j.ijheatmasstransfer.2008.06.016.

[25] Adkins D.R., Andraka C.E., Bradshaw R.W., Goods S.H., Moreno J.B., Moss T.A., "Mass Transport, Corrosion, Plugging, and Their Reduction in Solar Dish/Stirling Heat Pipe Receivers" , SAND96-1493C , IECEC 1996 Washington DC , Aug 1,1996

[26] Rosenfeld, John H., Ernst, Donald M., Lindemuth, James E., Sanzi, James L., Geng, Steven M., and Zuo, Jon, "An Overview of Long Duration Sodium Heat Pipe Tests", AIP Conf. Proc. 699, 140 (2004), DOI:10.1063/1.1649568

[27] Martin, J. J.; Reid, R. S., –Refractory Metal Heat Pipe Life Test—Test Plan and Standard Operating Procedures", Marshall Space Flight Center, Marshall Space Flight Center, Alabama, NASA/TP—2010–216452, Dec 2010.

[28] Merrigan, M., Dunwoody, W., Lundberg, L., –Heat Pipe Development for High Temperature Recuperator Application", Journal of Heat Recovery Systems, Volume 2, Issue 2, 1982, Pages 125-135, ISSN 0198-7593, 10.1016/0198-7593(82)90040-6.

[29] Baturkin, Volodymyr, Vladilen Zaripov, and Charles E. Andraka, –Development of Advanced Capillary Porous Structures of High Temperature Heat Pipes for Solar Receivers For Dish/Stirling Systems", 14th International Heat Pipe Conference (14th IHPC), Florianópolis, Brazil, April 22-27, 2007

[30] Moss T.A., "Building, Testing, and Post Test Analysis of Durability Heat Pipe #6" , SAND2002-0703 , Mar 1,2002

[31] Baturkin, V., and Moreno, J.B., –Study Of Structural and Mechanical Properties of Metal Felt Wicks Intended for High Temperature Heat Pipes - Solar Receivers", Proceedings of 12th International Heat Pipe Conference, Moscow, Russia, May 19-24 2002.

[32] Baturkin, V, —Development of Heat Pipes' Capillary Structures for Solar Recievers", IPP Project T1-0113-UA, National technical University of Ukraine, Kyiv, 2004.

[33] Sharifi, N., Wang, S., Bergman, T. L., and Faghri, A., 2012, "Heat pipe-assisted melting of a phase change material," International Journal of Heat and Mass Transfer, 55(13), pp. 3458-3469.

This page intentionally left blank

APPENDIX A: PCM PROPERTIES CONSIDERED

Material	Melting Point* (°C)	Heat of Fusion (kJ/kg)	Density [L/S] (kg/m^3)		Volumetric Storage Density (x10^6 kJ/m^3)		Thermal Conductivity (W/m·K)		Material Compatibility	Coefficient of Thermal Expansion (10^{-6} K^{-1})	Phase Change Volumetric Expansion	Vapor Pressure at T_m (mmHg)	Comments	KSR vote
Desired	750-800	High	High		High		High		Haynes-230	Low	Low	Low		
			Solid	Liquid	Solid	Liquid	Solid	Liquid						
Na	98 [16]	113 [16]	953.3 [16]	928.2 [16]	0.108	0.105	128	-	See Comments	70 [26]	0.027 [16]	-	May ignite spontaneously above 115C when exposed to air. Sodium fires release sodium monoxide and sodium hydroxide gas, which can cause chemical/thermal burns	Bad melting point, low vsd
Al**	660 [08]	400 [08]	2558 [08]	2377 [08]	1.023	0.951	204.2 [08]	94	-	23.1 [26]	0.09 [08]	-		Bad melting point
LiH	683 [08]	2582 [08]	790 [08]	-	2.04	-	4.2	2.1	-	-	-	-		Bad melting point
LiF	848±2 [10], 832 [08]	1037.9 [10]	2100 [10]	1799 [10]	2.18	1.867	5.99 [10]	1.73 [10]	[10] pg 19	-	0.294 [10]	0.0089 [10]	Expensive and in short supply [03]; Liquid density is for salt at 967C; Solid density calculated using liquid density and expansion on phase change	Slightly high MP, but great vsd, good cond, but see Evan notes.(Cut 2nd round)
KF	856±3 [10]	508.1 [10]	2307 [10]	1910 [10]	1.172	0.971	-	0.61 ± 0.018 [25]	[10] pg 39	-	0.172 [10]	123.2	Vapor pressure is for salt at 1277C; Solid density calculated using liquid density and expansion on phase change	Slightly high MP, but great vsd, poor cond
KCl	776 [03]	315.3 [03]	2066 [03]	1506 [03]	0.651	0.475	8.6 [03]	4.5-5.7 [03]	[10] pg 73	110 [28]	0.2227 [10]	4.22 [10]	Significant vapor pressure [03] can be corrosive even to high nickel alloys [03]	Great vsd, great cond, but see Evan notes.
NaBr	747 [19]	253.7 [19]	3120	2342 [25]	0.792	0.594	-	0.490 ± 0.003 [25]	-	~150-160 [28]	0.2494	-		Fair vsd, but poor cond.
NaCl	801 [03]	482.3 [03]	2104 [10]	1553 [10]	1.015	0.749	1.59 [03]	0.80-1.00 [03]	[10] pg 58	~150-160 [28]	0.2606 [10]	6.22 [10]	Vapor pressure is for salt at 977C; Liquid density is for salt at 807C; Solid density calculated using liquid density and expansion on phase change; thermal expansion coefficient measured at	Perfect MP, good vsd, fair cond, but bad expansion.
$MgCl_2$	715 [08]	454 [08]	2240 [08]	1675 [10]	1.017	0.76	0.84 [10]	1.21 [10]	[10] pg 90	-	0.3046 [10]	7.69 [10]	Vapor pressure is for salt at 947C; Liquid density is for salt at 827C	Bad MP, good vsd, poor cond.
$CaCl_2$	772 [03]	255.8 [03]	2146 [03]	2066 [03]	0.549	0.528	8.6-9.1 [03]	4.5-5.7 [03]	[10] pg 97	-	0.09 [10]	0.0014 [10]	Vapor pressure is for salt at 847C	Fair vsd, good cond, but NaCl better (Cut 2nd round).
Li_2CO_3	725 [08]	605 [08]	2200 [08]	1826[10]	1.331	1.105	1.47 [10]	1.97 [10]	[10] pg 111	205.11 [27]	0.69 [10]	8.5 [10]	Liquid density is for salt at 747C	Bad MP, great vsd, fair cond.
Na_2CO_3	858±1 [10]	280.5 [10]	2372 [10]	1968 [10]	0.665	0.552	1.31 [10]	1.84 [10]	[10] pg 122	224.66 [27]	0.162 [10]	7.8 [10]	Gives off toxic fumes when strongly heated, created problems if TES rupture occurs; If contaminated with $Mg(OH)_2$, oxichloride cement (MgOC1) may form [03]; Liquid density is for salt at 867C	Slightly high MP, fair vsd, fair cond, see Evan notes.
K_2CO_3	891 [03]	199.9 [10]	2264 [10]	1892 [10]	0.453	0.378	1.7 [03]	L1.7 [03]	[10] pg 133	216.68 [27]	0.164 [10]	0.23 [10]	Liquid density is for salt at 907C; Solid density calculated using liquid density and expansion on phase change	High MP, fair vsd, fair cond.
Li_3AlF_6	786 [14]	540 [14]	-	-	-	-	-	-	-	-	-	-		Not enough data.
$Na_2B_4O_7$	743	-	1730	-	-	-	-	-	-	-	-	-		Not enough data.
H755	755 [12]	466 [12]	2160 [12]	-	1.007	-	0.589 [12]	-	-	-	-	-		Slightly low MP, good vsd, poor cond, but NaCl a bit better all around, except expansion on NaCl bad!
NaK-78	–12.5 [16]	122.4 [16]	898.6 [16]	876.7 [16]	0.11	0.107	-	23.2 [17]	See Comments	70 (Na) 83 (K) [26]	0.025 [16]	1.00 [17]	Values for Thermal Conductivity and Vapor Pressure are for NaK at 100C; Boiling Point: 785C; Reacts explosively with water to form hydrogen, potassium hydroxide and sodium hydroxide; Reacts with air to form potassium superoxide, which can react explosivel	MP way low, see Evan notes.
Al-0.13Si†**	579 [08]	515 [08]	2553 [08]	2445 [08]	1.325	1.259	180 [08]	70 [08]	-	22.2 (Al) 5.1 (Si) [26]	-	-	Al-13.5Si	Bad MP, good vsd, excellent cond..
LiF-0.20CaF2†	766 [11]	815 [13]	2680 [13]	2100 [13]	2.184	1.712	3.8 [15] - 4 [13]	1.6 [13] - 1.7 [15]	-	0.287 [15]	0.216 [13]	-	LiF-42.2CaF2	Slightly low MP, excellent vsd, fair cond, see Evan notes on LiF. (Cut 2nd round)
LiF-0.22CaF2	766 [14]	750-760 [14]	-	-	-	-	-	-	-	-	-	-	LiF-8.57CaF2	Not enough data.
KF-0.14MgF2†	778 [11] 770 [14]	420-440 [14]	-	-	-	-	-	-	-	-	-	-	KF-14.9MgF2; k measured for solid at melting point	Not enough data.
LiF-0.25MgF2	740-748 [PD]	-	-	-	-	-	2.9 (MgF2) 5.3 (LiF) [24]	1.73 (LiF) [10]	-	-	-	-	MgF2-44.9LiF; k measured for solid at melting point	Slightly low MP, not enough data.
LiF-0.33MgF2†	746 [07], 740 [06][14], 742 [11]	550-560 [14]	-	-	-	-	2.9 (MgF2) 5.3 (LiF) [24]	1.73 (LiF) [10]	-	-	-	-	MgF2-45.8LiF; k measured for solid at melting point	Slightly low MP, guess vsd fair (need density), fair-good cond. (Cut 2nd round)
LiF-0.17MgF2	746 [05][08]	947 [08]	2630 [08]	-	2.49 [08]	-	2.9 (MgF2) 5.3 (LiF) [24]	1.73 (LiF) [10]	-	-	-	-	LiF-33MgF2; k measured for solid at melting point	Slightly low MP, good vsd, fair-good cond. (Cut 2nd round)
Cu-0.30Si†	803 [08]	196.8 [08]	6600 [08]	3100 (Cu), 2570 (Si) [25]	1.298 [08]	-	353-386 (Cu) [26] 52, 43, 36 (Si) [23]	157.18, 161.86, 164.35 (Cu) [22] 23, 22, 22 (Si) [23]	-	16.6 (Cu) 5.1 (Si) [26]	-	-	Cu-16Si; From PD (hyperlinked), eutectic point looks to be closer to Cu-0.33Si; k for Cu (s)measured at 20C, 300C, 600C, Cu(l) 1083, 1127, 1177; k for Si measured at 20C.	Perfect MP, excellent vsd, stunning cond. Ref [8] says this is one the best alloys for heat storage, and is 20% Si and 803C MP. Ratio density and cond accordingly? Vsd based on 6600 kg/m^3.
Cu-0.36Si	803 [08]	196.8 [08]	6600 [08]	3100 (Cu), 2570 (Si) [25]	1.298 [08]	-	353-386 (Cu) [26] 52, 43, 36 (Si) [23]	157.18, 161.86, 164.35 (Cu) [22] 23, 22, 22 (Si) [23]	-	16.6 (Cu) 5.1 (Si) [26]	-	-	Cu-20Si; k for Cu measured at 20C, 300C, 600C; k for Si(s) measured at 700C, 800C, 900C;	Perfect MP, excellent vsd, stunning cond. Same as above material, so picked above (Cut 2nd round).
NaF-0.32CaF2†	810 [11][14]	520-560 [14]	-	1948 (NaF), 2520 (CaF2) [25]	-	-	11.7 (CaF2) [21]	1.15 ± 0.028 (NaF)[25]	-	~140 (NaF) [29], 19.7-22.2 (CaF2) [26]	-	-	NaF-46.7CaF2	Good MP, good vsd, good cond. Ref 4 says florides expensive and in short supply. (Cut 2nd round)
KF-0.15CaF2†	780 [11], 782 [14]	450 [14]	-	1910 (KF), 2520 (CaF2) [25]	-	-	11.7 (CaF2) [21]	-	-	19.7-22.2 (CaF2) [26]	-	-	KF-19.2CaF2	Good MP, good vsd, good cond. Ref 4 says florides expensive and in short supply. (Cut 2nd round)
Mg-0.48Si†	910 [08]	774.6 [08]	-	1584 (Mg), 2570 (Si) [25]	-	-	52, 43, 36 (Si) [23]	23, 22, 22 (Si) [23]	-	5.1 (Si) 25 (Mg) [26]	-	-	Mg-44.4Si	Bad MP, good vsd, good cond.
Mg/Ca (84/16)†	790 [08]	272.1 [08]	1380 [08]	1584 (Mg) [25]	0.377 [08]	-	(Mg) 201(Ca) [26]	-	-	25 (Mg) 22.3 (Ca) [26]	-	-		Bad MP, fair vsd, good cond.
Si-0.35Cu-0.28Mg†	750 [03], 770 [08]	422.9 [08]	4150 [08]	2570 (Si), 3100 (Cu), 1584 (Mg) [25]	1.755	-	52, 43, 36 (Si) [23] 353-386 (Cu) 159 (Mg) [26]	157.18, 161.86, 164.35 (Cu) [22]	-	15.1 (Si) 6.6 (Cu) 25 (Mg) [26]	0.041 [08]	-	Cu-32.8Si-20.6Mg; k for Cu measured at 20C, 300C, 600C; k for Si(s) measured at 700C, 800C, 900C; k for Mg measured at 20C	Slightly low MP, great vsd, excellent cond.
NaF-0.22CaF2-0.13MgF2	745 [14]	510 [14]	-	1948 (NaF), 2520 (CaF2) [25]	-	-	61, 16.5, 11.7 (CaF2) [21] 4-15 (MgF2) [20]	1.15 ± 0.028 (NaF)[25]	-	~140 (NaF) [29], 19.7-22.2 (CaF2) [26]	-	-	NaF-32.7CaF2-20.6MgF2; k for CaF2 measured at 88C, 200C, 320C; thermal expansion coefficients for CaF2 represent range from 80-200C	Slightly low MP, good vsd, excellent cond. Ref 4 says florides expensive and in short supply. (Cut 2nd round)
NaF-0.14CaF2-0.09MgF2	745 [08][04]	574 [08]	2760 [08]	1948 (NaF), 2520 (CaF2) [25]	1.58 [08]	-	61, 16.5, 11.7 (CaF2) [21] 4-15 (MgF2) [20]	1.15 ± 0.028 (NaF)[25]	-	~140 (NaF) [29], 19.7-22.2 (CaF2) [26]	-	-	NaF-23CaF2-12MgF2; k for CaF2 measured at 88C, 200C, 320C; thermal expansion coefficients for CaF2 represent range from 80-200C	Slightly low MP, great vsd, excellent cond. Ref 4 says florides expensive and in short supply. (Cut 2nd round)
NaF-0.15KF-0.22MgF2†	798 [11]	-	-	1948 (NaF), 1910 (KF) [25]	-	-	4-15 (MgF2) [20]	1.15 ± 0.028 (NaF)[25]	-	~140 (NaF) [29]	-	-	NaF-17.8KF-28.6MgF2	Perfect MP, not enough data.
KF-0.21LiF-0.07Na3AlF6-0.03Al2O3	750	-	-	1910 (KF) [25]	-	-	5.99 (LiF) [10]	1.73 (LiF) [10]	-	-	-	-	KF-24.5Na3AlF6-8.9LiF-4.5Al2O3	Slightly low MP, not enoudgh data.
Mg - 0.38Si - 0.06Zn†	800 [19]	314 [20]	-	1584 (Mg), 2570 (Si) [25]	-	-	159 (Mg) [26] 52, 43, 36 (Si) [23] 353-386 (Cu) 116 (Zn) [26]	22, 22 (Si) [23]	-	25 (Mg) 5.1 (Si) 29.7 (Zn) [26]	-	-	Mg-38Si-15Zn; k for Mg measured at 20C; k for Si(s) measured at 700C, 800C, 900C; no T given for k for Zn	Perfect MP, fair vsd, excellent cond.

PCM Table References

#	Author(s)	Title	Publication Year	Publisher
1	Belen Zalba, Jose Marin, Luisa F. Cabeza, Herald Mehling	Review on thermal energy storage with phase change: materials, heat transfer analysis and applications	2003	Applied Thermal Engineering
2	-	Survey of Thermal Storage for Parabolic Trough Power Plants	2000	NREL
3	Joseph Alario, Robert Kosson, Robert Haslett	Active Heat Exchange System Development For Latent Heat Thermal Energy Storage	1980	NASA/DOE
4	PK Nag	Power Plant Engineering	2008	McGraw-Hill
5	CL Segaser	Survey Of Solar Thermal Energy Storage Subsystems For Thermal/Electric Applications	1978	ORNL
6	Cohen, Barry M., and Richard E. Rice	NAOH-Based High Temperature Heat-of-Fusion Thermal Energy Storage Device	1978	IECEC
7	John R. Gintz	Advanced Thermal Energy Storage Conept Definition Study for Solar Brayton Power Plants	1976	Boeing Engineering and Construction
8	C.E. Birchenall	Heat Storage In Alloy Transformations	1979	NASA/DOE
9	A Borucka	Survey and Selection of Inorganic Salts for Application to Thermal Energy Storage	1975	USRDA
10	Janz, G.J., C.B. Allen, N.P. Bansal, R.M. Murphy, R.P.T. Tomkins	Physical Properties Data Compilations Relevant to Energy Storage II. Molten Salts: Data on Single and Multi-Component Salt Systems	1979	NSRDS/ RPI
11	Janz, G.J., C.B. Allen, J. R. Downey Jr., R.P.T. Tomkins	Physical Properties Data Compilations Relevant to Energy Storage I. Molten Salts: Eutectic Data	1978	NSRDS/ RPI
12		PCM Products	2011	PCM Products
13	Wicher, R. P., Solomon, A. D., Drake, J. B., Williams, P. T.	Thermal Analysis of Heat Storage Canisteres for a Solar Dynamic, Space Power System	1988	ORNL
14	J. D. Whittenberger and A. K. Misra	Identification of Salt-Alloy Combinations for Thermal Energy Storage Applications in Advanced Solar Dynamic Power Systems	1987	Journal of Materials Engineering

15	Toutnier, Jean-Michel, El-Genk, Mohamed S,	Bellows-Type Accumulators for Liquid Metal Loops of Space Reactor Power Systems	2006	
16	BASF	Technical Data Sheet: Sodium-Potassium Alloy (NaK)	2003	BASF
17	Fernandez, Renedo, Perez, Carcedo, Manana	Advances In Phase Change Materials For Thermal Solar Power Plants Quality	2010	EA4EPQ
18	Kotz, John C., Treichel, Paul M., Townsend, John	Chemistry & Chemical Reactivity, Volume 2	2009	Thomson Brooks/Cole
19	Farkas, D., Birchenall, C.E.	New Eutectic Alloys and Their Heats of Transformation	1985	Meallurgical and Materials Transactions A
20	-	Magnesium Fluoride (MgF2) windows and lenses	-	Alkor
21	-	Calcium Fluoride (CaF2) Physical & Chemical Properties	-	Corning
22	Cagran, Claus	Thermal Conductivity and Thermal Diffusivity of Liquid Copper	2000	Istitut fur Experimentalphysik
23	-	Basic Mechanical and Thermal Properties of Silicon	-	Virginia Semiconductor, Inc.
24	M Martinex-Sanchez	The Feasibility of Using MgF2 For Phase Change Heat Storage In A Spacecraft Solar Thermal Power System	2010	MIT
25	-	Density of Molten Elements And Representative Salts	-	Fermi National Accelerator Laboratory
26	-	Engineering Toolbox	-	-
27	Liu, Q., Lange, R.	New Density Measurements On Carbonate Liquids And The Partial Molar Volume of the CaCO3 Component	2003	Springer-Verlag
28	Fang, Z.	Thermal expansion of ionic materials at high temperatures	2007	Journal of Applied Physics
29	Lagu, M., Dayal, B.	The equation of state and the thermal expansion of NaI and NaF	1974	Journal of Physics C: Solid State Physics

PCM table Comments

*-Many of the compounds given are not eutectic formulations, and thus do not have a single melting point (rather, melting occurs over a range of temperatures); therefore, this presents problems such as reduced performance of the Stirling engine. While a temperature range won't necessarily cause harm to the engine, this is a drawback to these compounds. A melt range beyond 50 C should likely be avoided.

**-Aluminum PCMs react with high nickel alloys (In625 and H230) like those used as containment material. Therefore, there might be a problem with Al-Si alloys. Wait for confirmation on this from Chuck/Nate.

***-Compositions are given in wt% if listed as whole numbers (i.e. 40/60) and given in mol% if listed as fraction (i.e. 0.4/0.6). If not clear, then entered as wt%.

Nitrate salts undergo a complex series of decomposition reactions, some irreversible, at temperatures above 500C. The production of these reactions (e.g. alkali oxides, nitrogen oxide gases) are corrosive to metallic system components

Non-green values without reference(s) listed in cell are calculated from other values for which references are given.

Green- Indicates properties for which data was given in the previous spreadsheet or for which data was found online, but for which there was no source in the literature. It appears that some of these values may be for eutectic alloys of these compounds; however, this has not been verified

Reference 10 includes tables for ks and kl in increments of 100K. For materials in which the spreadsheet indicates [10] as the source for the value of Ks, the closest value to T_m was used to determine an estimate.

†-designates that alloy is eutectic or close to eutectic. Values for eutectic mixture vary in sources, so values that were within ~±0.01 mol fraction of the eutectic composition as identified by various sources are counted as eutectic. If there was no close-to-eutectic ratio listed in the previous spreadsheet, but one could be identified in the literature or phase diagrams, it was added.

††- Isostatic powder compacting is a mass-conserving shaping process. Fine metal particles are placed into a flexible mould and then high gas or fluid pressure is applied to the mould. The resulting article is then sintered in a furnace. This increases the strength of the part by bonding the metal particles. This manufacturing process produces very little scrap metal and can be used to make many different shapes.

Melting temperatures with [PD] references are ranges for melting for non-eutectic binary mixtures. They are based on phase diagrams (accessible by clicking link in name). The lower bound is the estimated melting point for one solid; the upper bound is the estimated melting point for the other.

According to Dave Gill, "metals, upon melting, may see a slight decrease in conductivity. However, salts, when melting, see a substantial increase in conductivity, 10x to 50x." (Chuck). Based on the behavior of copper, it appears metals experience a decrease in k upon phase change, but k increases gradually after melting. While the decrease may be as much as 50%, in the case of pure copper, k is still far higher than that of salts. [22]

Reference 11 includes a table of eutectic salt mixtures that fit the melting point range of 750-800 C.

Could non-eutectic/far-from-eutectic compositions present problems with separation upon multiple cycles due to density differences and disparate melting points?

Although rare, eutectic composition does not always imply congruent melting. In the event that subcooling exists, phase change may not occur simultaneously. Thus, phase separation is in some situations possible even for eutectic compositions.

DISTRIBUTION:

(Distributed by electronic copy only)

Rich Diver
Diver Solar
1112 Monte Largo NE
Albuquerque, NM 87123

Ray Erbeznik
Infinia Corp.
300 W 12th Street
Ogden, UT 84404

Maury White
Infinia Corp.
300 W 12th Street
Ogden, UT 84404

David Miklosi
Stirling Biopower
275 Metty Drive
Ann Arbor, MI 48103-9444

Nate Siegel
Bucknell University
1 Dent Drive
Lewisburg, PA 17837

Amir Faghri
Department of Mechanical Engineering,
School of Engineering
University of Connecticut
191 Auditorium Rd., Unit 3139
Storrs, CT 06269

Volodymyr Baturkin
National Technical University of the Ukraine
(Kyiv Polytechnic Institute)

Judith Gomez, PhD
National Renewable Energy Laboratory
Concentrating Solar Power Department
15013 Denver West Parkway
Golden, CO 80401

Mark Mehos
National Renewable Energy Laboratory
Concentrating Solar Power Department
15013 Denver West Parkway
Golden, CO 80401

Joseph W. Stekli
U.S. Department of Energy
Solar Energy Technology Program
950 L'Enfant Plaza SW
Washington, DC 20585

Jesse Gary
U.S. Department of Energy
Solar Energy Technology Program
950 L'Enfant Plaza SW
Washington, DC 20585

Ranga Pitchumani
U.S. Department of Energy
Solar Energy Technology Program
950 L'Enfant Plaza SW
Washington, DC 20585

Tommy Rueckert
U.S. Department of Energy
Solar Energy Technology Program
950 L'Enfant Plaza SW
Washington, DC 20585

Sandia National Laboratories Distribution

MS0721	Marjorie Tatro	6100
MS0836	Roy Hogan	1514
MS0968	K. Scott Rawlinson	2611
MS1033	Charles Hanley	6112
MS1084	Subhash Shinde	1746
MS1104	Juan Torres	6120
MS1127	William J. Kolb	6123
MS1127	Cheryl Ghanbari	6123
MS1127	Brian Iverson	6123
MS1127	Clifford Ho	6123
MS1127	James Pacheco	6123
MS1127	Tim Moss	6123
MS1127	David D. Gill	6123
MS1127	Chuck Andraka	6123
MS1127	Julius Yellowhair	6123
MS0899	Technical Library	9536


Sandia National Laboratories